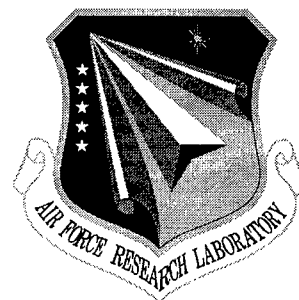AFRL-SN-RS-TR-1998-44
Interim Technical Report
April 1998

MULTICHANNEL RECEIVER CHARACTERIZATION FOR ADAPTIVE ARRAY APPLICATIONS PHASE 3: ASSESSMENT OF THE BISTATIC RECEIVER TESTBED AS A MEASUREMENT TOOL FOR CLUTTER PHENOMENOLOGY

W.L. Simkins, Proprietor

William L. Simkins

APPROVED FOR PUBLIC RELEASE; DISTRIBUTION UNLIMITED.

19980618 100

**AIR FORCE RESEARCH LABORATORY
SENSORS DIRECTORATE
ROME RESEARCH SITE
ROME, NEW YORK**

Although this report references limited documents (*), listed on page 6-2, no limited information has been extracted.

This report has been reviewed by the Air Force Research Laboratory, Information Directorate, Public Affairs Office (IFOIPA) and is releasable to the National Technical Information Service (NTIS). At NTIS it will be releasable to the general public, including foreign nations.

AFRL-SN-RS-TR-1998-44 has been reviewed and is approved for publication.

APPROVED: *Elaine Kordyban*

ELAINE KORDYBAN
Project Engineer

FOR THE DIRECTOR: *Robert G. Polce*

ROBERT G. POLCE, Acting Chief
Rome Operations Office
Sensors Directorate

If your address has changed or if you wish to be removed from the Air Force Research Laboratory Rome Research Site mailing list, or if the addressee is no longer employed by your organization, please notify AFRL/SNRD, 26 Electronic Pky, Rome, NY 13441-4514. This will assist us in maintaining a current mailing list.

Do not return copies of this report unless contractual obligations or notices on a specific document require that it be returned.

REPORT DOCUMENTATION PAGE

Public reporting burden for this collection of information is estimated to average 1 hour per response, including the time for reviewing instructions, searching existing data sources, gathering and maintaining the data needed, and completing and reviewing the collection of information. Send comments regarding this burden estimate or any other aspect of this collection of information, including suggestions for reducing this burden, to Washington Headquarters Services, Directorate for Information Operations and Reports, 1215 Jefferson Davis Highway, Suite 1204, Arlington, VA 22202-4302, and to the Office of Management and Budget, Paperwork Reduction Project (0704-0188), Washington, DC 20503.

1. AGENCY USE ONLY *(Leave blank)*	2. REPORT DATE	3. REPORT TYPE AND DATES COVERED
	April 1998	Interim May 95 - Dec 96

4. TITLE AND SUBTITLE

MULTICHANNEL RECEIVER CHARACTERIZATION FOR ADAPTIVE ARRAY APPLICATIONS; PHASE 3: ASSESSMENT OF THE BISTATIC RECEIVER TESTBED AS A MEASUREMENT TOOL FOR CLUTTER PHENOMENOLOGY

6. AUTHOR(S)

William L. Simkins

5. FUNDING NUMBERS

C   - F30602-95-C-0015
PE - 62702F
PR - 4506
TA - 16
WU - 1S

7. PERFORMING ORGANIZATION NAME(S) AND ADDRESS(ES)

W. L. Simkins, Proprietor
2600 Waldron Rd
Camden NY 13316

8. PERFORMING ORGANIZATION REPORT NUMBER

N/A

9. SPONSORING/MONITORING AGENCY NAME(S) AND ADDRESS(ES)

AFRL/SNRD
26 Electronic Pky
Rome NY 13441-4514

10. SPONSORING/MONITORING AGENCY REPORT NUMBER

AFRL-SN-RS-TR-1998-44

11. SUPPLEMENTARY NOTES

AFRL Project Engineer: Elaine Kordyban/SNRD/(315) 330-4481

12a. DISTRIBUTION AVAILABILITY STATEMENT

Approved for public release; distribution unlimited

12b. DISTRIBUTION CODE

13. ABSTRACT *(Maximum 200 words)*

This report describes Phase 3 of a multi-phase effort to develop an existing multichannel receiver into a multi-use bistatic testbed. It presents an assessment of the adaptive array receiver's utility for investigating clutter phenomenology and defines two experiments that demonstrate its capabilities.

14. SUBJECT TERMS

Surveillance, Bistatic Radar, Terrain Clutter

15. NUMBER OF PAGES

68

16. PRICE CODE

17. SECURITY CLASSIFICATION OF REPORT	18. SECURITY CLASSIFICATION OF THIS PAGE	19. SECURITY CLASSIFICATION OF ABSTRACT	20. LIMITATION OF ABSTRACT
UNCLASSIFIED	UNCLASSIFIED	UNCLASSIFIED	UL

TABLE OF CONTENTS

1.0 INTRODUCTION

The Department of Defense has an interest in the detection of low visibility threats. One approach, currently under investigation by Rome Laboratory, involves the development of Advanced Offboard Bistatic Technology for improved detection and tracking of low visibility targets. For the purpose of this report, low visibility targets are those with an inherently low radar cross section (RCS) or those that use natural features to reduce or mask the targets return. Stealth technology is an example of the first type while the aircraft using terrain shadowing or vehicles using the attenuation and clutter of a vegetation canopy are examples of the second type. The sensor technology involves the development of a modern adaptive multichannel bistatic radar system for use with cooperative and non-cooperative transmitters.

A goal of an adaptive ground-based or airborne surveillance radar system is to have optimum or near-optimum detection and tracking of weak targets in the presence of strong clutter and interference while maintaining a low false alarm rate. Several adaptive techniques have been suggested to meet these criteria including adaptive space-time processing [1,2], adaptive multipath and jamming cancellation [3,4] and adaptive beamforming [5]. The performance of all these techniques depends on the target-to-noise ratios (T/N), the clutter-plus-interference-to-noise ratios (C+I/N) and the spatial-temporal amplitude and correlation statistics of the target, the clutter and the interference. Radar measurements and experiments are required to demonstrate the performance of these techniques and to quantify the target and clutter statistics that determined each technique's limitations. The objective of this effort is to assist Rome Laboratory in creating a fundamental multichannel measurement capability to perform multidomain adaptive radar experiments.

W. L. Simkins is performing a multi-phase effort to assist Rome Laboratory in the development of the existing multichannel receiver into a multi-use bistatic testbed. The first phase report [6] provided an evaluation of the existing system with recommendations for improving performance. The second phase recommended the procedures and post-A/D algorithms for maintaining real-time calibration of the adaptive array receiver [7]. The third task, presented in this report, presents an assessment of the existing adaptive array receiver's utility for investigating clutter phenomenology and defines two experiments that demonstrate the capabilities of RL's adaptive receiver's capabilities.

Section 2 presents a brief review of the existing adaptive array receiver and its auxiliary equipment. Section 3 review the results of tests using the array and derives two descriptive

parameters of the array receiver: the gain-aperture product and the sensitivity factor. These parameters are used with the bistatic radar range equation to allow quick assessment of the array's performance with a given host transmitter.

Section 4 discusses the use of the existing bistatic facility for the measurement of radar cross section (RCS) and propagation. Several programs for investigating the clutter and propagation were proposed and two experiments were defined. The first experiment addresses the problem of detecting targets within a vegetation canopy. The experiment provides a method for simultaneously measuring the propagation through the vegetation and the clutter backscatter from the vegetation. The output of such an experiment would provide the information needed to determine the effectiveness of using vegetation to screen moving vehicles and other assets while also providing the sensor requirements needed to reduce this effectiveness.

The second proposed experiment addresses the terrain shadowing problem and the potential of using transportable or fixed bistatic adjunct receivers to increase the coverage in the regions illuminated predominately by diffracted energy. An experiment was defined that allows the simultaneous measurement of the bistatic and monostatic propagation characteristics, the bistatic and monostatic radar cross section of the test aircraft and the bistatic and monostatic clutter return from the diffraction region. Other related experiments were also briefly mentioned.

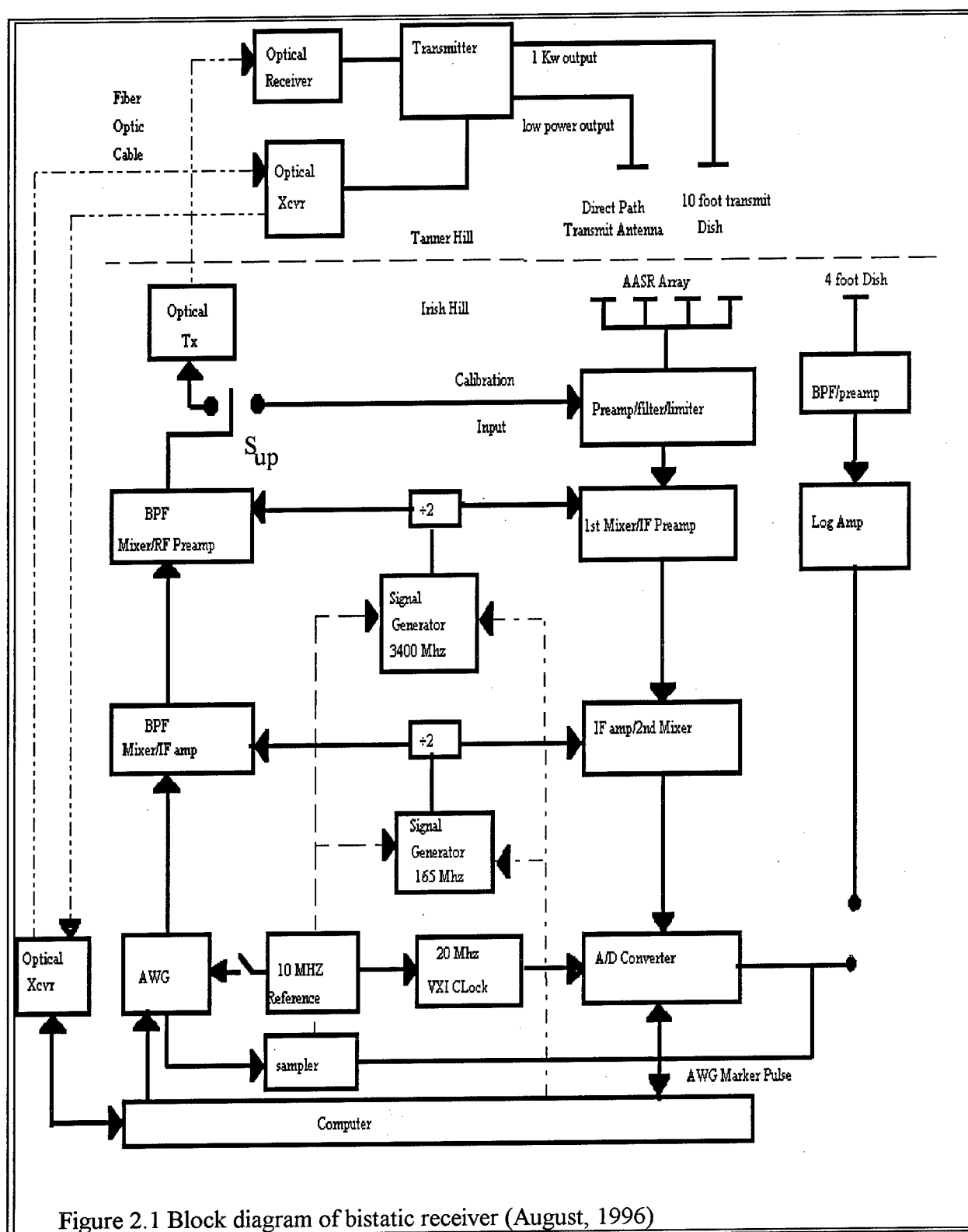This report concludes with a summary and conclusions in Section 6.0.

2.0 REVIEW OF THE BISTATIC FACILITY

This section provides an overview of the bistatic receiver and its associated equipment located at the Newport test site from 1995 through September 1997. Figure 2.1 shows the configuration of the Newport testbed during 1996. The system consists of several subsystems for waveform generation, control and data collection.

The Intel-based Radisys VXI controller provides the user interface and control of the system and the DOS-based storage system for data. The Arbitrary Waveform Generator (AWG) provided a programmed waveform on a 5 MHz carrier to the up-converter. The output of the upconverter is manually transferred to either a calibration port for internal calibration or to the optical transmitter. The optical signal is received and demodulated at the transmitter site on Tanner Hill. This S-Band signal is provided to either the low power transmitter for array compensation measurements or to the high power transmitter for most experiments. The output of the bistatic receiver array is down-converted to a 5 MHz carrier, digitized and stored in an internal high speed buffer memory. The data is then transferred to the Dos-based storage in the controller. System coherence is maintained in the converter oscillators and the digitizers by locking all clocks to a 10 MHz reference.

A second optical system for remote control purposes was under development and was not used during 1996. Also shown is an auxiliary receiver using a 4 foot dish and a log amplifier. This subsystem is used during synchronization when the bistatic system is used with another host transmitter.

In 1997, the high power transmitter subsystem was moved to a location on Irish Hill. The 10 foot dish and pedestal were placed in a concrete pad on the northeast side of the main building with the transmitter placed in a nearby location within the building. The low power CW transmitter remained on Tanner Hill and used a sheltered 10 foot dish to provide a calibration signal. Use of the low power and high power transmitter required manually switching the optical output from the receiver at the optical junction box. Another change in 1997 is the use of a standard PC and MXI interface board in place of the Radisys controller.
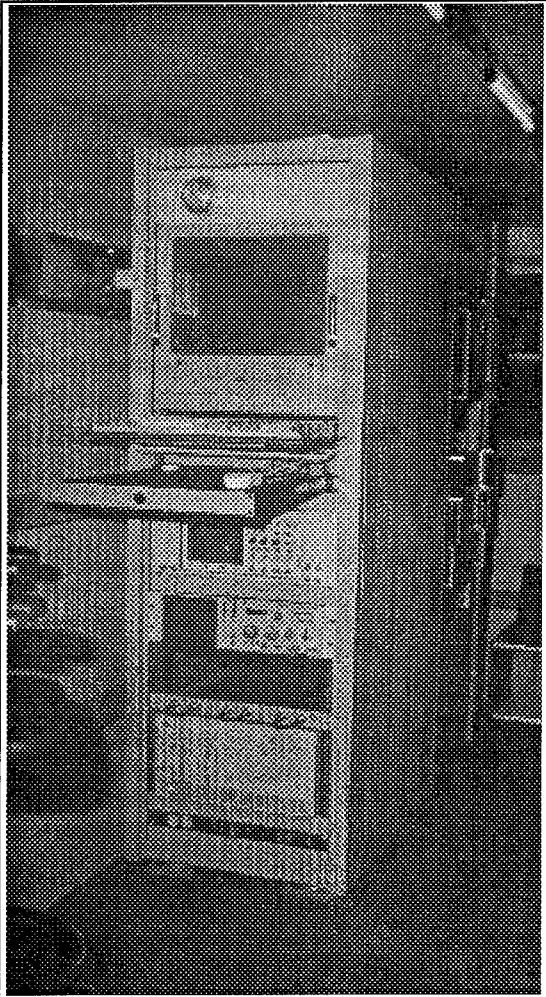
Figure 2.1 Block diagram of bistatic receiver (August, 1996)

2.1 Waveform Generation and Up-Converter Subsystem

The waveform generation and up-converter subsystem provides calibration waveforms as well as radar transmitter signals for use at the Newport site. The waveform is generated using an HP 8770A Arbitrary Waveform Generator (AWG), a programmable device that provides waveforms with frequencies up to 50 MHz via a high-speed 125 MHz, 12 bit Digital-to-Analog Converter (D/A). Figure 2.2 shows the user console that houses the AWG in the lower shelf and the user console and test equipment in the higher shelves. The high dynamic range and high degree of oversampling allow the AWG to provide a high quality signal centered at 5 MHz. The manufacturer [9] sites phase linearity of +/- 5 degrees, harmonic distortion less that 50 dBc and single-sideband (SSB) phase noise of less than -120 dBc at a 10 kHz offset. Within the 2.5 MHz to 7.5 MHz passband of the receiver, the signal-to-phase-noise ratio (S/N) at the AWG output is approximately 60 dB. The AWG is programmed to provide different waveforms via a software interface developed by Rome Research, Inc. System coherence is maintained by phase-locking the AWG's internal sampling clock to the system's 10 MHz reference oscillator.

Figure 2.2 User console with computer display, AWG and test equipment

The AWG signals are up-converted to S-Band using the same LO sources as those used in the receiver. Figure 2.3 presents a block diagram of the up-converter fabricated by Rome Lab personnel. The noise contributed by the up-converter components include both thermal and phase noise components. The S/N limitation of the thermal noise components is approximately 80 dB, over 10 dB below the AWG noise level, and does not significantly impact the test signal's quality.

The primary phase noise contributors are the oscillator used to create the signal, the oscillator used to provide the A/D sampling clock and the two local oscillators used in frequency conversion. When the same oscillators are used in both the transmitter up-conversion and receiver

down-conversion, the phase noise power is a function of the short-term stability of these oscillators and the time delay t_d between transmission and reception. The power in the phase noise sidebands S(f) and the total phase noise N_{phase} can be given as [10,11]

$$S(f_m) = 4\left(\frac{\Delta f}{f_m}\right)^2 [\sin(\pi f_m t_d)]^2$$

$$N_{phase} = \int_0^{B_{coh}} S(f_m) df_m$$

where f_m is the offset frequency of the phase modulation, Δf is the frequency deviation in Hz and B_{coh} is the noise bandwidth of the receiver after coherent processing. For stable crystal oscillators, the fractional frequency deviation $(\Delta f/f_m)$ is typically less that 10^{-5} at $f_m = 10$ kHz dropping to a floor of less than 10^{-7} at $f_m = 100$ kHz and higher offset frequencies. For the calibration measurements discussed in the next section, the time delay through the up-converter, calibration cables and the receiver is approximately 4 usec. For a noise bandwidth of 5.6 MHz, this results in a phase noise power of less than 60 dB below the carrier. With the stable VHF and microwave oscillators used in the system, the phase noise corresponding to such a small time delay is insignificant. However, at longer ranges or when another transmitter source is used, phase noise will become more important.

2.2 Optical and transmitter subsystem

The Newport test site consists of two hilltop sites that are approximately 6600 feet apart and 330 feet above the intervening valley. Optical fiber cable is available for the transmission of

Figure 2.3 Up-Converter Block Diagram (October 1995) [6,8]

Figure 2.4 Optical transmitter [6,8]
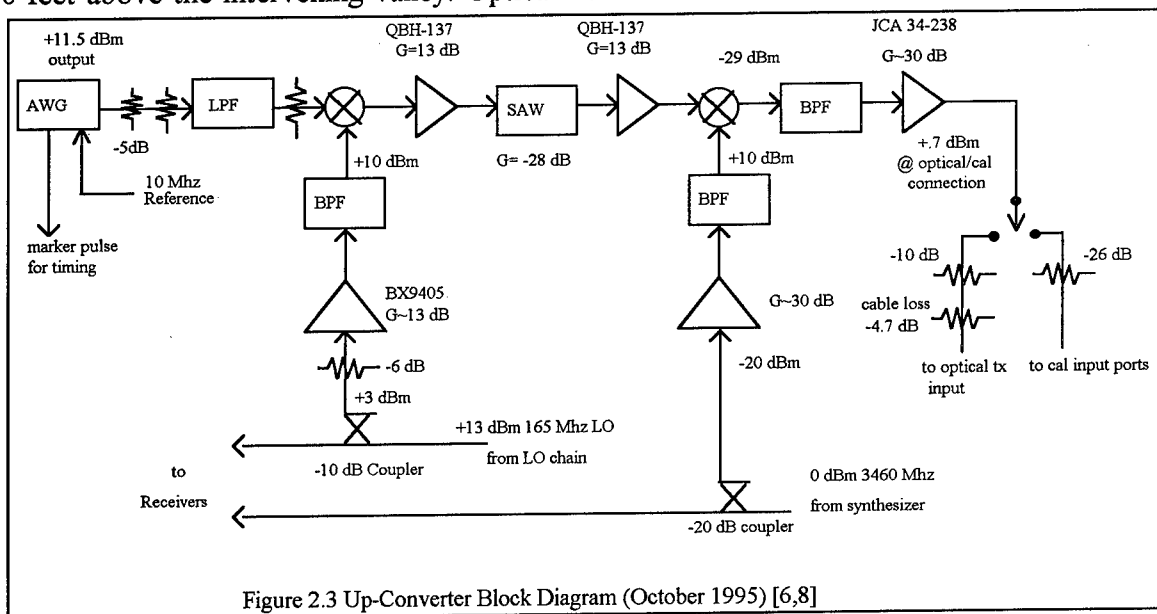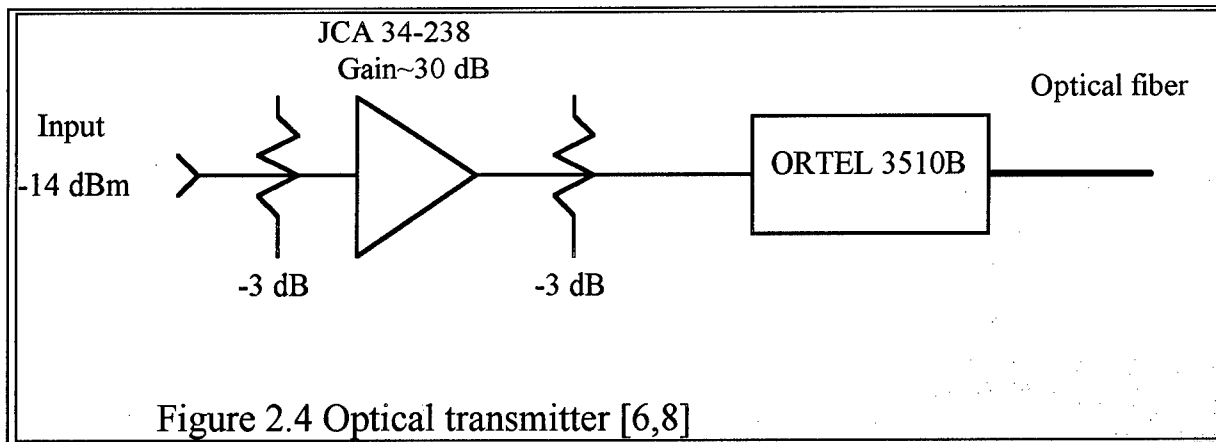
timing and RF signals between the Tanner Hill and Irish Hill sites. The bistatic testbed shelter is located on Irish Hill and uses this optical link to sent transmit signals to a TWT transmitter located on Tanner Hill. The optical transceiver system consists of an Ortel 3510B optical transmitter and an Ortel 4508 optical receiver. A second optical transceiver system was installed in 1996 to provide timing and remote control of the recently installed 1 kW (peak) pulsed transmitter and to allow remote monitoring of the parameters of the pulse transmitter, cw transmitter and the transmit antenna.

At S-Band, the maximum linear signal is obtained at the optical receiver with an input of +10 dBm into the optical transmitter. The loss in the optical system is approximately -52 dB and the measured signal-to-noise ratio (S/N) ratio at the output is approximately 45 dB. The measurement of optical loss is highly dependent on the quality and cleanliness of the optical cable connectors. Repeated removals and reinsertion's of the fiber cable can easily provide several dB of change in the observed optical loss and S/N.

The third-order intercept point of the optical system is listed at over +25 dBm. This is not important for typical radar waveforms such as gated CW, pseudorandom phase codes and LFM, because such waveforms provide only one frequency at a given instant in time. Such waveforms can be transmitted at levels as high as +10 dBm input with good fidelity. However, tests requiring the simultaneous transmissions of multiple frequency waveforms require a compromise in total input power and fidelity.

Both low power (<25 watts) and high power pulsed TWT's have been discussed for use in future experiments. The low power transmitter is used primarily with a fixed antenna for receiver calibration and equalization. The 1 kW (peak) pulsed TWT uses a steerable 10 foot dish to provide signals for local experiments.
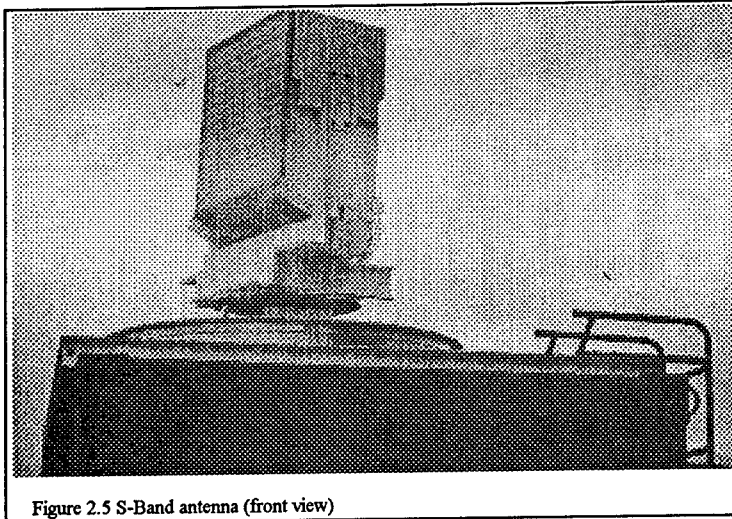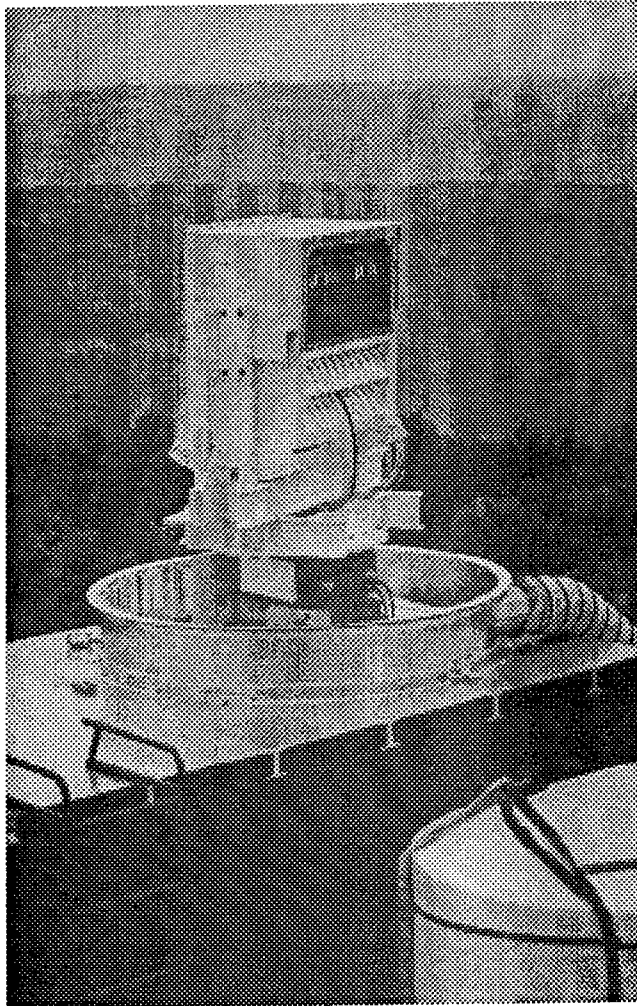
Figure 2.5 S-Band antenna (front view)

2.3 Antenna and Receiver Subsystem

Figures 2.5 and 2.6 show the front and rear view of the antenna respectively while Figure 2.7 shows the antenna with the radome in place. The antenna is a passive device consisting of 16 columns, each column consisting of 16 patch stripline antennas coupled with stripline couplers. The antenna is mounted on a pedestal that provides digital-controlled azimuth steering of plus or minus 180 degrees. The elevation angle is positioned manually from -8 degrees to + 8 degrees. In 1996, the front third of the radome plastic was replaced with clear Lexan to reduce loss.

Figure 2.8 shows a block diagram of the preamp assembly and the first mixer located in the receiver. The RF preamp modules are mounted near the column outputs to reduce the line lengths and the associated losses contributing to system noise figure. The hardline cable used between the antenna and the preamp assembly was carefully matched to preserve the gain and phase matching of the array outputs. Adjustable lines are also included to allow compensation of the phase differences in the preamp assemblies.

The preamp assembly's limiter is used to prevent damaging signal levels into the receiver while an SPDT switch provides further protection and reduces the interference

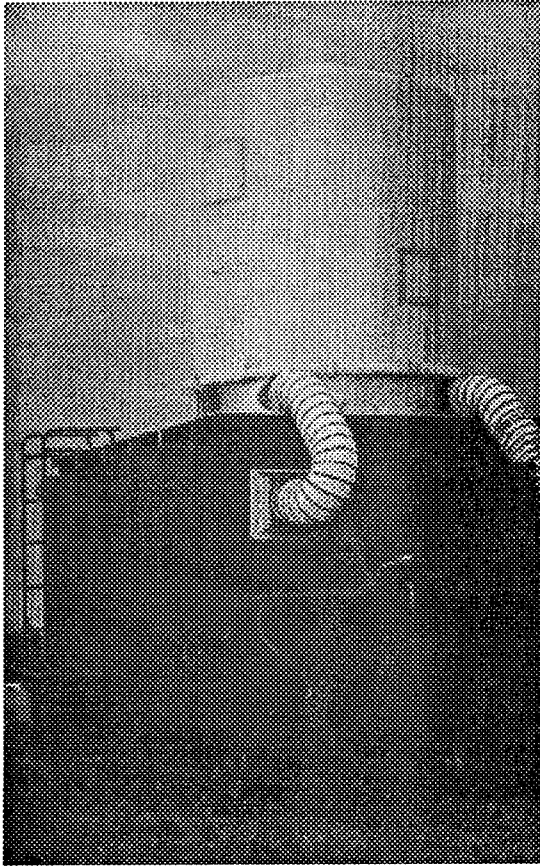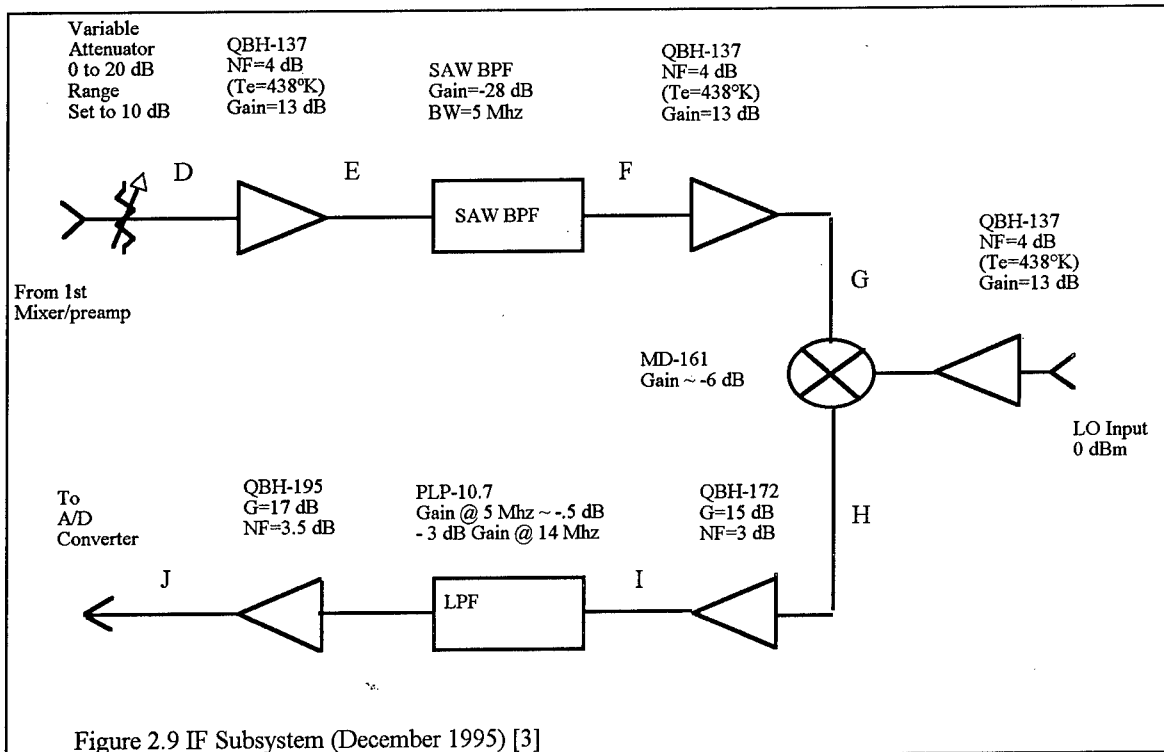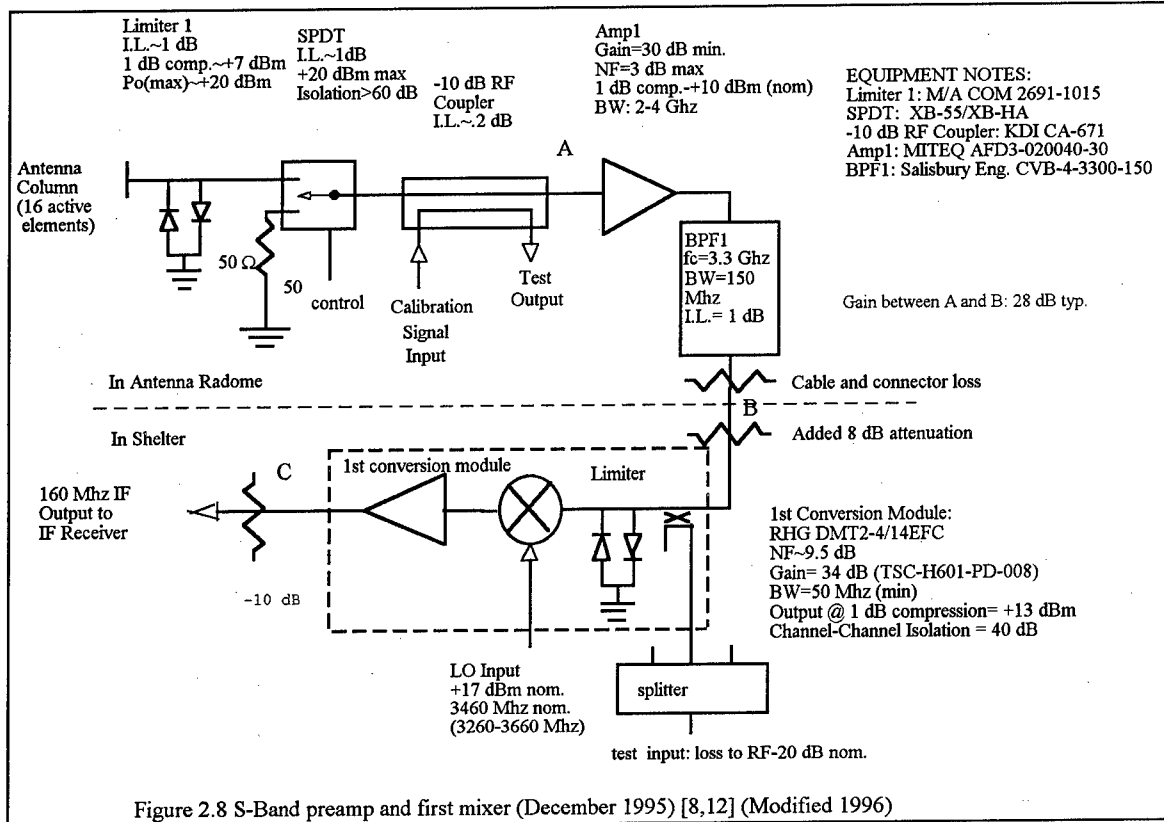Figure 2.6 S-Band antenna (rear view)
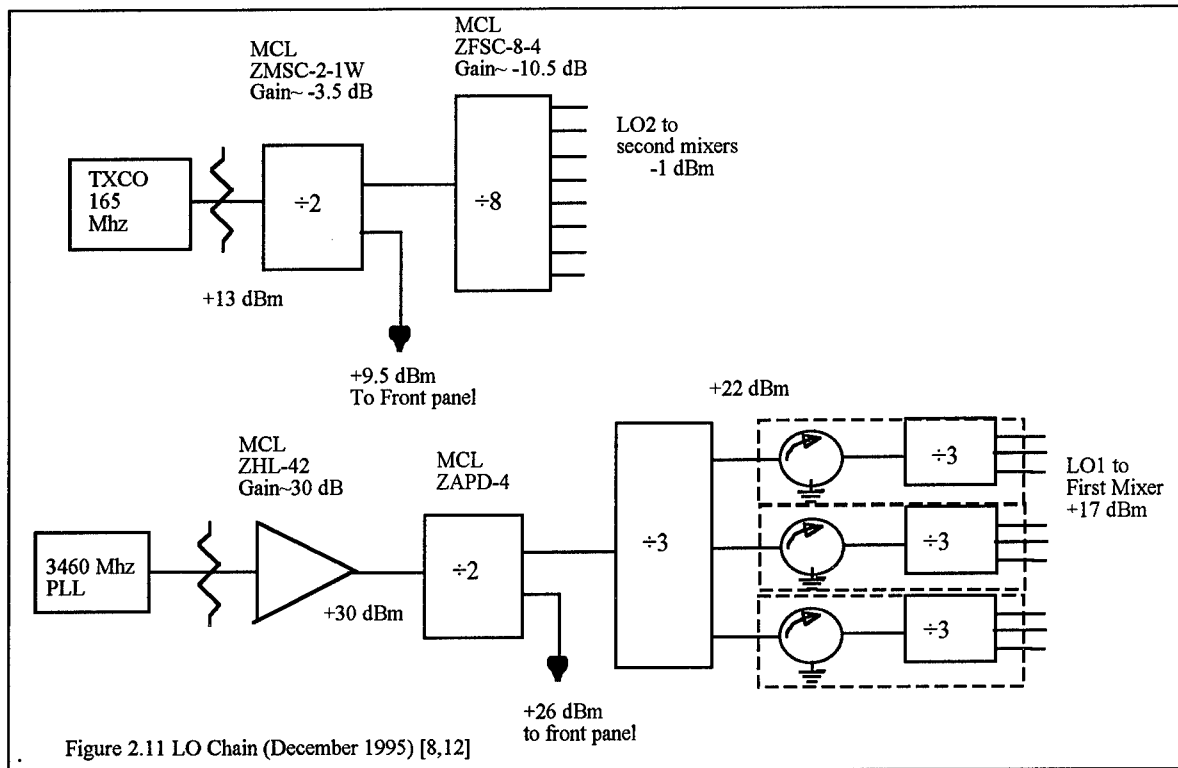
Figure 2.7 S-Band antenna with radome

from external signals during calibration tests. The -10 dB coupler allows the injection of a known signal for calibration and provides the test outputs used to form uniformly weighted sum and difference channels for setup and diagnostics.

When the system is in the calibration mode, the calibration signal is fed via hardline from the shelter to the antenna compartment where it is split into 16 channels, each channel associated with a column receiver. The measured loss and phase shift from the optical/cal switch to the coupler input are given in Table 2.2. The nominal loss is 18.2 dB at 3300 MHz with a (-.2/+.1 dB) variation from column to column. The variation over the 5 MHz band is within +/- .2 dB. The peak deviation of the phase from linear was less than 1 degree for each column.

Table 2.2 Measured amplitude loss in calibration cable

Column	3295 MHz Loss(dB)/phase(deg)	3300 MHz Loss(dB)/phase(deg)	3305 MHz Loss(dB)/phase(deg)
1	-18.1 / -32.1	-18.0 / -83.5	-17.9 / -134.5
2	-18.3 / -36.0	-18.3 / -86.7	-18.2 / -138.4
3	-18.3 / -48.1	-18.2 / -99.0	-18.2 / -151.2
4	-18.2 / -52.2	-18.2 / -102.8	-18.1 / -154.8
5	-18.1 / -22.8	-18.0 / -73.4	-17.9 / -125.6
6	-18.3 / -20.3	-18.1 / -71.5	-17.9 / -123.5
7	-18.3 / -46.8	-18.2 / -98.0	-18.1 / -149.8
8	-18.2 / -10.9	-18.2 / -61.8	-18.2 / -113.7
9	-18.3 / -28.1	-18.3 / -78.8	-18.2 / -130.8
10	-18.3 / -14.8	-18.3 / -65.7	-18.2 / -117.5
11	-18.4 / -30.3	-18.3 / -81.1	-18.2 / -132.8
12	-18.4 / -21.6	-18.3 / -72.5	-18.2 / -124.3
13	-18.4 / -32.3	-18.3 / -82.4	-18.2 / -133.7
14	-18.4 / -28.7	-18.3 / -79.7	-18.2 / -131.7
15	-18.4 / -25.8	-18.3 / -76.8	-18.2 / -128.5
16	-18.4 / -31.9	-18.3 / -82.5	-18.2 / -134.4

Figure 2.8

Limiter 1
I.L.~1 dB
1 dB comp.~+7 dBm
Po(max)~+20 dBm

SPDT
I.L.~1dB
+20 dBm max
Isolation>60 dB

-10 dB RF
Coupler
I.L.~.2 dB

Amp1
Gain=30 dB min.
NF=3 dB max
1 dB comp.-+10 dBm (nom)
BW: 2-4 Ghz

A

EQUIPMENT NOTES:
Limiter 1: M/A COM 2691-1015
SPDT: XB-55/XB-HA
-10 dB RF Coupler: KDI CA-671
Amp1: MITEQ AFD3-020040-30
BPF1: Salisbury Eng. CVB-4-3300-150

Antenna
Column
(16 active
elements)

50 Ω

50

control

Calibration
Signal
Input

Test
Output

BPF1
fc=3.3 Ghz
BW=150
Mhz
I.L.= 1 dB

Gain between A and B: 28 dB typ.

In Antenna Radome

Cable and connector loss

B

In Shelter

Added 8 dB attenuation

1st conversion module

Limiter

C

160 Mhz IF
Output to
IF Receiver

-10 dB

1st Conversion Module:
RHG DMT2-4/14EFC
NF~9.5 dB
Gain= 34 dB (TSC-H601-PD-008)
BW=50 Mhz (min)
Output @ 1 dB compression= +13 dBm
Channel-Channel Isolation = 40 dB

LO Input
+17 dBm nom.
3460 Mhz nom.
(3260-3660 Mhz)

splitter

test input: loss to RF-20 dB nom.

Figure 2.8 S-Band preamp and first mixer (December 1995) [8,12] (Modified 1996)

Figure 2.9

Variable
Attenuator
0 to 20 dB
Range
Set to 10 dB

QBH-137
NF=4 dB
(Te=438°K)
Gain=13 dB

SAW BPF
Gain=-28 dB
BW=5 Mhz

QBH-137
NF=4 dB
(Te=438°K)
Gain=13 dB

D

E

SAW BPF

F

From 1st
Mixer/preamp

QBH-137
NF=4 dB
(Te=438°K)
Gain=13 dB

G

MD-161
Gain ~ -6 dB

LO Input
0 dBm

To
A/D
Converter

QBH-195
G=17 dB
NF=3.5 dB

PLP-10.7
Gain @ 5 Mhz ~ -.5 dB
- 3 dB Gain @ 14 Mhz

QBH-172
G=15 dB
NF=3 dB

H

J

LPF

I

Figure 2.9 IF Subsystem (December 1995) [3]

2-8

Figure 2.11 LO Chain (December 1995) [8,12]

The preamps have a nominal noise figure of 3 dB and a minimum gain of 30 dB. The 4-pole bandpass filter has a bandwidth of 150 MHz to reduce the system's response to the image signals and the out-of-band interference. Matched lengths of hardline cable is used to transfer the 16 column signals from the bandpass filters located in the preamp assembly to the receivers located within the shelter.

An earlier interim document [6] characterized the receiver and made recommendations for improving the system's linear dynamic range. For a modest increase in noise figure (.85 dB), the linear dynamic range for third order distortion could be increased close to the limitation provided by the "10 "effective bits" advertized for the 11 bit A/D converter [13]. Since the system is used where the experimental parameters can be chosen to meet the S/N limitations and where the linear dynamic range is important, then the trade-off between linear dynamic range and noise figure is reasonable.

As shown in Figure 2.9, the receiver gain was reduced by 8 dB, providing the suggested improvement in dynamic range. The figure also presents a block diagram of the if receiver. Most of the receiver's selectivity is provide by the surface acoustic wave (SAW) bandpass filter. Figure 2.10 presents the filter shape and general characteristics of these devices. The -3 dB bandwidth is nominally 5.6 MHz and a nominal rejection between -45 and -50 dB is obtained at offset

frequencies from 4.8 MHz to 80 MHz. The Mini-Circuits PLP-10.7 low-pass filter provides additional selectivity, reducing adjacent channel signals and noise beyond 15 MHz .

The isolation between channels is limited by the LO chain (Figure 2.11). The RHG 3-channel mixer/preamps specify a 40 dB minimum isolation between the three channels contained within each module. The circulator and splitter provides an additional 40 dB of isolation between different modules. The 8-way splitter and the MD-161 mixers used in the second down conversion provide a minimum of 50 dB isolation.
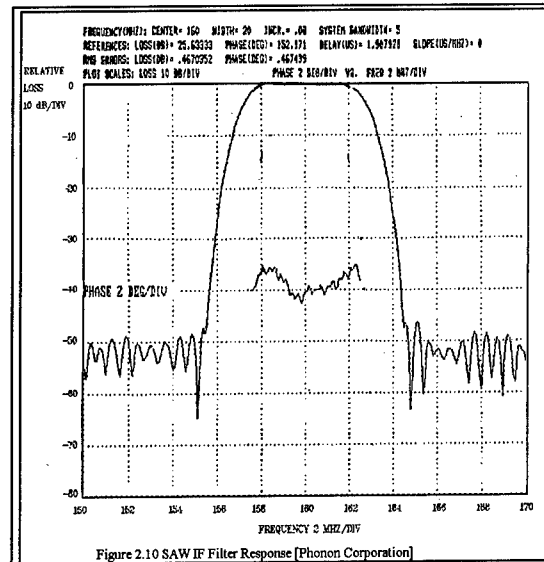

Figure 2.10 SAW IF Filter Response [Phonon Corporation]

2.1.4 The A/D Converter, Digital and Timing subsystems

The original digital subsystem is a VXI-based system consisting of a Radisys 486-based controller, 8 dual-channel analog-to-digital (A/D) converters, VXI-based hard drives and an interface for logging GPS time. Each A/D converter is a HP E11429B digitizer, a dual-channel 12-bit VXI-based device capable of performing 20 million sample/second. Table 2.4 lists some of the specifications of these dual-channel converters. The harmonic distortion, at 61 dB down from a full scale signal, and the total noise and distortion of the A/D converters from all sources, at 59 dB down, were less than that created by the receiver's final amplifier. The timing of the bistatic receiver consists of several oscillators used for frequency conversion, A/D conversion and other timing. Coherence is maintained by locking the oscillators to a 10 MHz reference.

The manufacturer claims that the 1 volt, 50 ohm single-ended range provides the most linear A/D performance. The Least Significant Bit (LSB) signal specifies a sinusoidal signal at the A/D converter with an rms value equal to the LSB. For an 12 bit A/D converter operated in its +/- 1 volt bipolar mode (11 bits plus sign), the digital output has a range from +2046 for a 1.023 volt peak input to -2045 for a -1.0225 volt peak input. (-2048, -2047, -2046 and 2047 either indicate overload or are not used.) The LSB corresponds to 1.023/2047 = .0005 volts. An LSB signal within a rms value of .0005 volts into 50 ohms would have an average power of -53 dBm.

Each digitizer contained a 512 Kword (1 MByte) buffer memory that can be partitioned for multiple recordings using software. The recorded data can then be transferred to the Radisys DOS-based drive or to a VXI drive or processor.

In 1997, a standard PC and a MXI interface board replaced the Radisys controller to provide more flexibility, more data storage and a better user interface. A software interface to a VXI drive was also developed for faster HP Local Bus transfers. The advertised transfer rate of the buffer memory data to other devices was 2-4 MWord/second via the VME bus and 20-40 MWord/second via the HP Local bus. However, the observed transfer rates were significantly less. During September 1997, the observed HP local bus transfer rate from the digitizers to the VXI disk drive was on the order of 20 MBytes/second while the transfer of the data from the VXI drive to the DOS drive was on the order of 64 KBytes/sec. Development is continuing on this software to improve speed and reliability. The transfer rate from the digitizers to the DOS drive using the Rome Research software was in the order of 10 KBytes/second. While this transfer is slow, it is very reliable and was used to record the data presented in this report.

Table 2.4 Specifications of the HP E1429A/B 20 MSa/s 2-Channel Digitizer [13]

Resolution:	12 Bits (11 Bits + sign) -2045 to +2046 on-scale readings
Sample rate:	20 Million samples/sec
Effective number of bits: (4.5.2; 4.1.3)***	10.3 bits typical for 500 kHz signal 9.8 bits typical at 10 MHz signal
Harmonic distortion: (4.4.2.1)***	-64 dB THD at 500 kHz (THD includes 2nd through 6th harmonic) -61 dB THD at 10 MHz
Signal-to-Noise Ratio:** (4.5.1)***	62 dB at 500 kHz 59 dB at 10 MHz
Differential Nonlinearity: (4.4.1.2)***	1 LSB
Integral Nonlinearity: (4.4.3)***	2 LSB
Memory:	512K readings (1 MByte) Partitionable in to 2^n segments where n = 0 to 7
Input Voltage Range:	-0.10225 to 0.10230 V / 50 ohm -0.2045 to 0.20460 V / 50 ohm -0.51125 to 0.51150 V / 50 ohm -1.0225 to 1.02300 V / 50 ohm
Analog Bandwidth: (4.6.1)***	> 50 MHz (1 V range) > 40 MHz (other ranges)
Cross-talk: (4.11)***	-80 dB, DC to 10 MHz
Read-Out Speed:	
VME Bus	up to 2 M readings/sec (16 bit transfers) up to 4 M readings/sec (32 bit transfers)
Local Bus*	up to 20 M readings/sec (either channel separately) up to 40 M readings/sec (both channels interleaved)

* readings may be routed to Local Bus during digitization and simultaneously with recording in the internal memory
** includes noise, distortion and all other undesired effects as defined in IEEE 1057
*** refers to sections in IEEE Standard 1057

3.0 Calibration and System Performance

An interim report [7] discussed the issues in calibrating the bistatic system. These issues included compensation for the phase and amplitude distortion for each channel, equalization of the channel-to-channel variations and calibration of the multi-channel receiver for the measurement of bistatic radar cross of clutter targets.

3.1 Overview

The existing S-Band multichannel receiver is to be used in performing bistatic experiments and concept evaluations in support of the Advanced Offboard Bistatic Technology effort. These bistatic experiments include the measurement of the bistatic RCS and spectra of natural and manmade structures, aircraft and vehicles, the measurement of the bistatic RCS and spectra of terrain clutter, sea clutter and weather clutter, the testing of multi-domain adaptive processes against jamming and clutter and the evaluation of the use of a bistatic adjunct receiver for strategic gaps filling or covert tactical use.

These tests can provide useful and repeatable information only if proper calibration is performed during the measurements. The term calibration is used in its most general sense. That is, calibration is a method for quantifying the observations and conditions of an experiment such that the experiment, when reproduced by others, will provide repeatable results. This not only requires that the equipment be calibrated such that the imperfections of the bistatic recording system are compensated for and powers, voltages, losses and gains are measured accurately. It also requires that the ground-truth associated with the measurement be recorded and the definitions used in creating the results be clearly and concisely presented.

For example, consider a measurement of the mean and distribution of homogeneous land clutter. The term "homogeneous" means that each cell within a region has some set of similar properties. While the concept is clear, the implementation is not standardized. Some might map the terrain into homogeneous areas based on physical features (local slope, vegetation, etc.) while others might create a map based on radar reflectivity statistics (mean, spread, correlation length). It is not obvious that the two maps would be the same. Thus, results using the first criterion may be of limited use to those interested in homogeneity based on the second criterion. Furthermore, if results were given without reference to the criterion used, the results are best considered antidotal. Therefore, to get calibrated and repeatable results, the ground truth and criterion used in the analysis must be part of the calibration process.

Target
σ_t

Illumination path parameters
$F_t \ L_{et} \ R_t$

ϑ

$\beta/2$ $\beta/2$

Echo path parameters
$R_r F_r \ L_{er}$

Θ_R

Θ_T

T

Transmitter.
$P_t G_t L_t$

R **baseline**

R
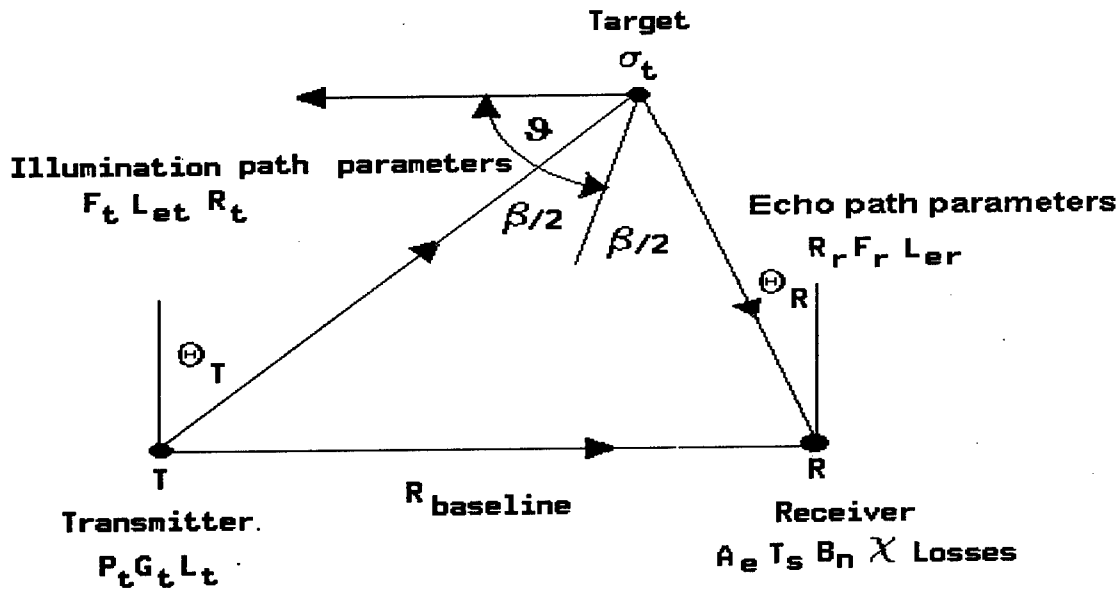
Receiver
$A_e \ T_s \ B_n \ X \ Losses$

Figure 3.1 Bistatic geometry

The type and nature of ground-truth data needed to quantify measurements are often interdisciplinary and are highly dependent on the factors that the analyst believes impacts the measurement results. This is especially true for clutter measurements where the RCS, Doppler and other echo characteristics are highly dependent on a variable natural environment. Therefore, the bistatic testbed can only provide the ability to record and tag a number of auxiliary data files that each experiment can redefine as needed.

However, the variables generally associated with the bistatic radar receiver and its associated equipment can be identified and the issues impacting the calibration of the bistatic system can be quantified. The radar range equations given in (3.1) and (3.2) provide the typical parameters of interest in a radar application.

$$(3.1) \ S = \left(\frac{P_t G_t(\theta_t, \phi_t)}{L_t} \right)\left(\frac{F_t^2}{4\pi R_t^2 L_{et}} \right)\left(\frac{\sigma_t}{1} \right)\left(\frac{F_r^2}{4\pi R_r^2 L_{er}} \right)\left[\left(\frac{\bar{A}_{col} N_{col}}{\bar{L}_{col} L_{wtr} \bar{L}_r} \right)\left(\frac{\bar{G}_r}{1} \right)\left(\frac{\Re N_p}{L_{wtr} L_{wtp}} \right) \right]$$

$$(3.2) \ \frac{S}{N} = \left(\frac{P_t G_t(\theta_t, \phi_t)}{L_t} \right)\left(\frac{F_t^2}{4\pi R_t^2 L_{et}} \right)\left(\frac{\sigma_t}{1} \right)\left(\frac{F_r^2}{4\pi R_r^2 L_{er}} \right)\left[\left(\frac{\bar{A}_{col} N_{col}}{\bar{L}_{col} L_{wtr} \bar{L}_r} \right)\left(\frac{\Re N_p}{\bar{L}_{comp} L_{wtr} L_{wtp}} \right)\left(\frac{1}{\kappa \bar{T}_s B_n L_{AD} L_{IQ}} \right) \right]$$

The terms are defined in Appendix A. Two parameters are defined in this report to allow a quick assessment of the bistatic receiver performance with a host transmitter. One parameter is the gain-aperture product *GA*

$$GA = \left[\left(\frac{\bar{A}_{col}}{L_{radome}\, \bar{L}_{col}\, \bar{L}_{r}} \right) \left(\frac{N_{col}}{L_{wta}} \right) \left(\frac{G_r}{L_{comp_s}} \right) \left(\frac{\mathcal{R}N_p}{\bar{L}_{collapse}\, L_{wtr} L_{wtd}} \right) \right]$$

which relates the power density at the face of the array to the output power of the processed signal.

The second term is the sensitivity factor $\mathcal{S}$

$$\mathcal{S} = \left[\left(\frac{GA}{G_r L_{comp}\, \kappa \bar{T}_s\, B_n L_{AD} L_{IQ}} \right) \right]$$

which relates the power density at the face of the array to the signal-to-noise ratio after processing.

The following sections will discuss these terms in more detail.

3.2 System Performance

For experiments involving the measurement of a manmade target or a clutter target, calibration involves establishing a relationship between the received signal and the target parameters. For the example of measuring target radar cross section, system calibration establishes a relationship between the received power and the target cross section. When combined with auxiliary information on the target description and aspect, repeatable measurements of target RCS can be performed. For detection experiments, calibration provides an accurate definition of the receiver components for experiment design, for data evaluation and for comparison with simulation results.

The bistatic receiver channels were characterized by their gain and group delay vs. frequency in two earlier reports [5,7]. The differences between the channels were small and a processing approach for equalizing the channels was proposed. Several recommendations and modifications were also proposed and some were implemented by Rome Lab personnel during 1996 and 1997. One of the recommendations was the reduction of receiver gains. This increased the linear dynamic range at the cost of a slight increase in system noise figure. Another change was the use of an additional A/D module to provide the system sample clock to the VXI backplane. Originally, the first A/D module was used to pass an external locked 20 MHz clock to the VXI modules. This resulted in a 3 sample delay between the sampling of the first module and the other 7 A/D modules. The use of the additional A/D module eliminated this 3 sample delay

Figure 3.2 Calibration setup. Gains shown for channel 1
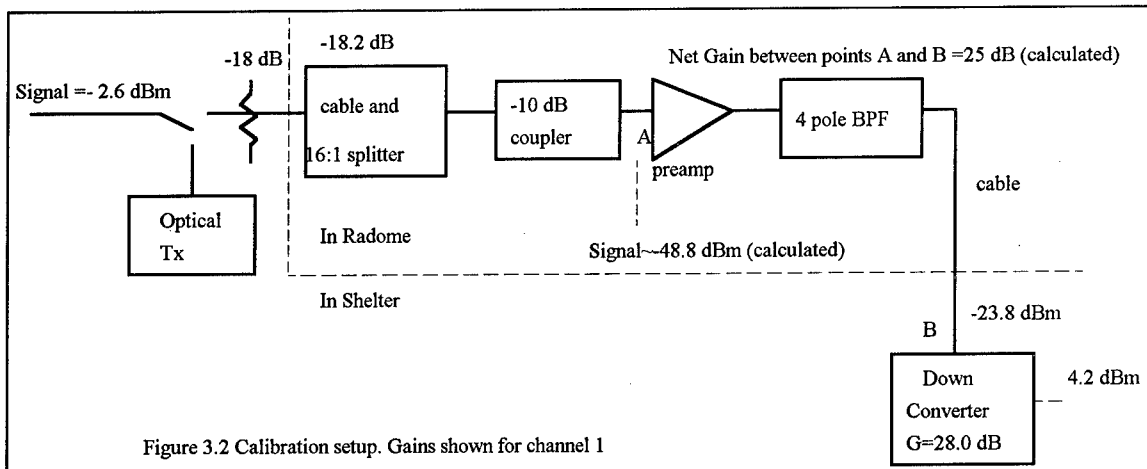
and reduced the constant differential delays between the channels to a fraction of the sample period.

Proposed algorithms and methods were presented for the calibration of the bistatic receiver in 1997. During the summer of 1997, these procedures were implement to demonstrate how that the bistatic receiver could be calibrated to provide consistent and repeatable results [35]. This section presents some of these measurements of the system performance and calibration to provide a basis for the development of the experiments.

Section 3.2.1 presents recent measurements updating the gains and losses within each analog receiver channel. Section 3.2.2 reviews the gains and losses in the standard signal processing functions such as matched filtering, Doppler processing, channel equalization and azimuth beamforming. Section 3.2.3 presents a discussion of the column array losses and the impact of multipath on their measurement. Measurement results are presented using the direct signal from the transmitter and the array parameters including its gain-aperture product GA and its sensitivity factor δ are presented. The section concludes with the results of an RCS measurement using a calibrated transponder and a comparison with the results with that predicted using the measured array parameters.

3.2.1 Analog Receiver Channels

Measurements of the current receiver gains were performed using the internal calibration loop. The internal calibration signals are used to confirm system performance during the initial system checkout, as a measurement and diagnostic tool for the receiver from the preamp through the A/D converter and to provide a clean waveform reference for use as a matched filter and compensation for intra-channel distortion [7]. Internal calibration measurements are performed using the closed loop given in Figure 2.1 of the previous section.

Figure 3.2 shows a simplified diagram of the calibration loop. The waveform is created by the AWG and upconverted to S-Band. The output of the upconverter is passed to the input of each column preamp via attenuation, a series of cables, a 16:1 splitter and a -10 dB coupler. The nominal calculated signal level at the input to each preamp (Point A) is -49 dBm with a signal-to-noise ratio of 53 dB. The gain of the channel receivers from the preamp input to the A/D converter input ranges from 50.2 to 55.5 dB with an average gain $\bar{G}_r$ of 54.3 dB. This compares with the system gains of 58.6 to 61.4 dB measured in 1995. Table 3.1 provides a list of the gains for each channel measured in September, 1997.

Channel	Gain A-B (dB)	Thermal Noise @A/D output (dBm)	AWG+Thermal Noise Noise @ A/D Output (dBm)	Noise at I/Q output (dBm)	Compensation Signal gain (dB)	Noise after Compensation (dBm)
1	53.5	-49.0	-47.5	-43.8	0	-43.8
2	54.2	-48.9	-47.4	-44.2	-.7	-44.9
3	54.4	-48.8	-47.3	-44.0	-.9	-44.9
4	53.1	-48.9	-47.4	-44.2	.4	-43.8
5	54.3	-49.0	-47.5	-44.1	-.8	-44.9
6	54.4	-48.9	-47.4	-44.2	-0.9	-45.1
7	55.6	-48.3	-46.8	-43.9	-2.1	-46.0
8	54.9	-47.8	-46.3	-43.9	-1.4	-45.3
9	55.6	-47.0	-46.5	-42.4	-2.1	-44.5
10	54.6	-48.1	-46.6	-44.0	-1.1	-45.1
11	55.5	-48.1	-46.6	-42.6	-2.0	-44.6
12	54.2	-48.8	-47.3	-44.3	-0.7	-45.0
13	54.4	-48.5	-46.9	-44.1	-0.9	-45.0
14	50.6	-51.8	-50.3	-46.9	+2.9	-44.0
15	54.3	-49.0	-47.5	-44.1	-0.8	-44.9
16	52.8	-49.2	-47.7	-45.3	+0.7	-44.6
avg.	54.3	-48.6	-47.2	-44.0	-----	-44.7

Table 3.1 Measured channel characteristics using internal calibration port

With the input terminated and no signal injected, the noise output from each channel ranged from -47 dBm to -51.8 dBm averaging -48.6 dBm. The average receiver noise temperature is given as

$$\bar{T}_e = \bar{T}_s - \bar{T}_{term}$$

where $\bar{T}_s$ is the average noise temperature referenced to the preamp input.

$$\bar{T}_s = \frac{\bar{N}_{in}}{\kappa B_n} = \frac{\bar{N}_{out}}{\kappa B_n \bar{G}_r}$$

and T_{term} is the temperature of the input termination that is assumed to have a temperature of 290°K. Using Boltzmann's constant $\kappa = 1.38 \times 10^{-20}$ mw/°K-sec, $B_n = 5.6$ MHz, $\bar{G}_r = 269153$ (54.3 dB) and $\bar{N}_{out} = 1.38 * 10^{-5}$, the average system noise temperature $\bar{T}_s = 663$ °K and the average receiver noise temperature $\bar{T}_e = 373$ °K. These values are close to those estimated in [7].

3.2.2 Signal Processing Gains and Losses

Figure 3.3 shows processing typical of a bistatic radar receiver. After A/D conversion, digital IF-to-quadrature detection is performed to provide an in-phase and quadrature (I/Q) representation of the signal. Channel-to-channel compensation equalizes the gain and group delay across signal bandwidth prior to matched filtering. For multi-pulse bursts, Doppler filtering can be performed. Beamforming provides the final coherent process before envelope detection. For track operations, the processing load can be reduced by processing only the Doppler filter and beam containing the test target. For search and detection tests, all filters and beams must be processed.

Most of the gains and losses in the digital processing can be calculated accurately from theory. In this report, the weights used in each process are normalized to provide unity noise gain. This approach equates the signal gains and losses with the respective gains and losses of signal-to-noise ratio. A review of the gains and losses are given in the following brief review using a 16 pulse burst of a linear frequency modulated (LFM) waveform as an example.

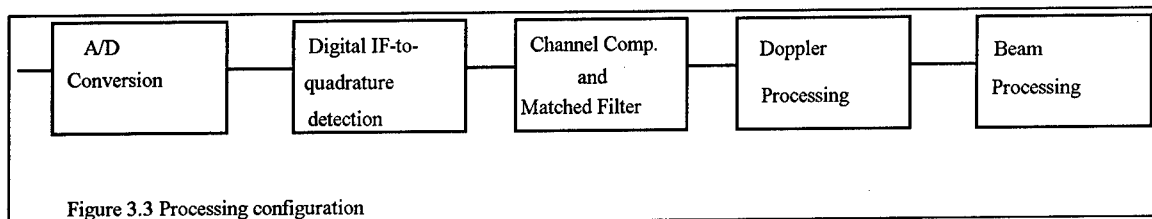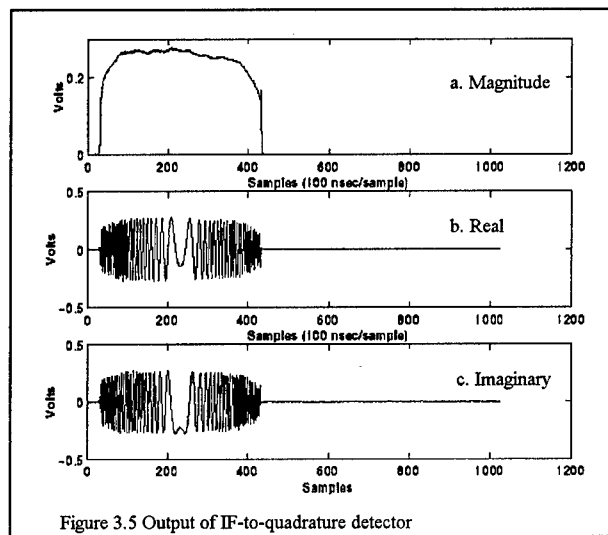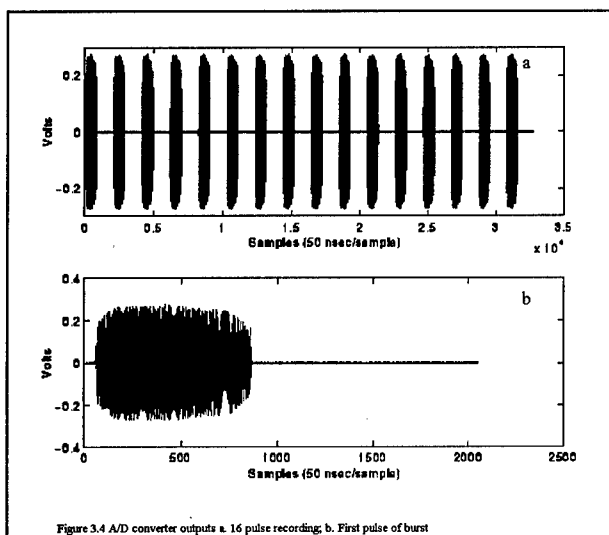| A/D Conversion	Digital IF-to-quadrature detection	Channel Comp. and Matched Filter	Doppler Processing	Beam Processing

Figure 3.3 Processing configuration

Figure 3.4 shows a record of the A/D converter output when using an LFM waveform with a bandwidth of 5 MHz and a pulse width of 40 microseconds. The waveform was generated by the AWG, upconverted to S-Band and passed to the receiver using the calibration port. The signal gain of the A/D converter is unity. However, the sampling and conversion processes add noise to the output. The two dominate sources of in-band noise are quantization noise and noise from aperture jitter. For a (b+sign) bit converter used with two's complement truncation, the standard deviation of the quantization noise is $\dfrac{2^{-b}}{\sqrt{12}}$ volts or .141 mv for b=11 [7,23]. The standard deviation of the noise due to aperture jitter has been estimated as $(.79*10^{-6})^{.5}$ = .89 mv for 5 MHz bandwidth signals [7,13]. Assuming the noises are uncorrelated, the total additive noise is .9 mv.

The S/N loss due to this noise is a function of the noise input level. The receiver gains have been set to provide an average noise level of -48.6 dBm into the converters. This level corresponds to an rms voltage of 1.15 mv or 2.4 quantums into the 50 ohms input impedance of the converter. A reasonable estimate of the S/N loss due to the conversion is given by [33]

$$L_{A/D} = 10\log(1 + \frac{\sigma_A^2}{\sigma_n^2}) = 10\log(1 + \frac{(.9)^2}{(1.15)^2}) = 2.1 dB.$$

Figure 3.5 presents the same recording after digital IF-to-quadrature detection. The digital IF-to-quadrature process used the Hilbert transform process given in several references [7,26-29]. Fourier transforms of twice the sample window are used to eliminate the increase in noise due to foldover. The signal gain of the digital IF-to-quadrature process was set to unity. However, the

Figure 3.4 A/D converter outputs a. 16 pulse recording; b. First pulse of burst

Figure 3.5 Output of IF-to-quadrature detector

S/N loss L_{IQ} is about 3 dB [7]. A comparison of the noise outputs for the A/D converter and quadrature detection in Table 3.1 and Figure 3.6 demonstrates this loss. The signal power at the A/D converter input and the quadrature output is +0.9 dBm. The noise output at the A/D converter output is -47.2 dBm, providing a peak signal-to-noise ratio of 48.1 dB. After quadrature detection, the noise is -44.1 dBm and the peak signal-to-noise ratio is 45.0 dB.

After quadrature detection, channel matching and equalization is performed by creating 16 filters to compensate for the difference in average gain and group delay within each channel as well as the amplitude and phase distortion within the passband [7]. A broadband signal such as a 5 MHz LFM is passed through the receiver and recorded. The amplitude and phase slope across the bandpass are compared to an ideal delayed reference and a filter is created to compensate for the differences. If $S_{ideal}(\omega)$ is the spectrum of the ideal signal and S_i is the measured signal from channel i, then, $H_i(\omega) = \left[\dfrac{S_{ideal}(\omega)e^{j\omega\tau_i}}{S_i(\omega)} \right]K_1$

where the scaling constant K_1 is given by

$$K_1 = \frac{\max|S_1(\omega)|}{\max|S_{ideal}(\omega)|}$$

and the estimate of the group delay τ_i is derived from the unwrapped phase estimates $\varphi(f_2)$ and $\varphi(f_1)$ at frequencies f_2 and f_1.

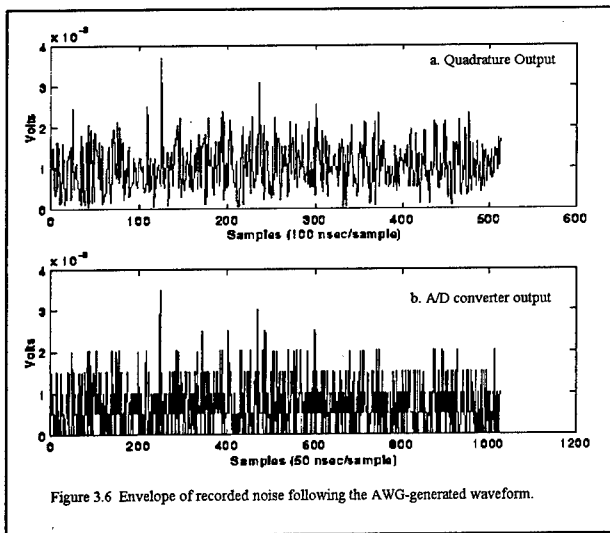$$\tau_i = \frac{\varphi(f_2) - \varphi(f_1)}{2\pi(f_2 - f_1)}$$

Figure 3.7 presents the general shape of the recorded signal's spectrum before and after compensation. As noted in the earlier reports [6,7], the distortion of the 16 channels is small across the 5 MHz bandpass. The compensation filter is stored and applied to subsequent recordings. Figure 3.8a presents the LFM waveform before compensation while Figure 3.8b shows the signal after compensation.
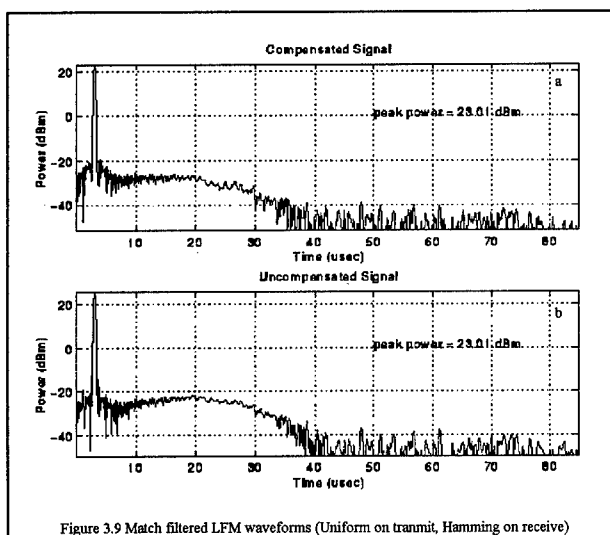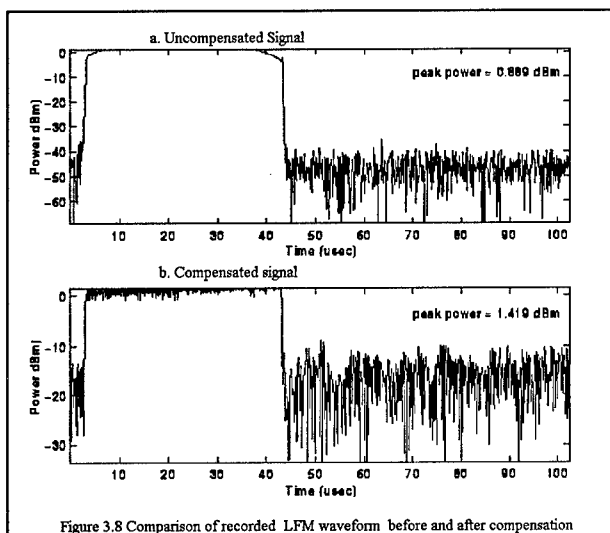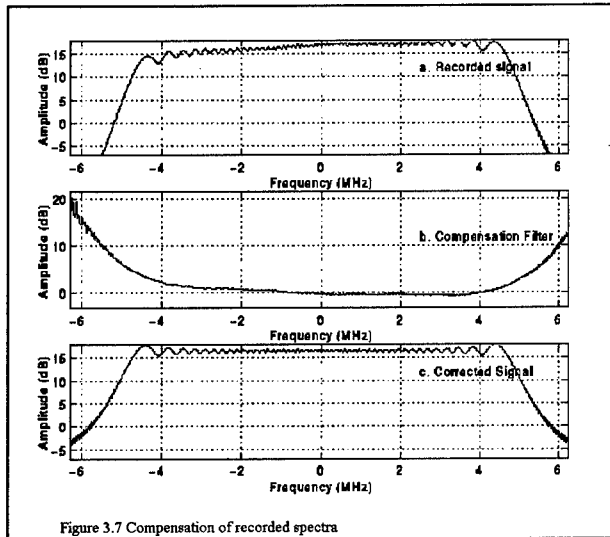

Figure 3.6 Envelope of recorded noise following the AWG-generated waveform.

Figure 3.7 Compensation of recorded spectra

Figure 3.8 Comparison of recorded LFM waveform before and after compensation

Two additional effects of the compensation process can be noted. First, the signal power is changed to reflect the equalization of the channel gain. Table 3.1 shows the signal gain/loss for the compensation filter for each channel. The average signal loss $\bar{L}_{comp}$ is .8 dB to provide a compensated gain of 53.5 dB in each channel. Second, the noise power has increased due to the compensation filter gain at the frequencies above 5 MHz. Since this noise is not within the passband of the signal, it is severely attenuated by the matched filter. This is illustrated by the comparison of the match filter outputs in Figure 3.9. While the signal has the same power in both the compensated and the uncompensated output, the noise (shown in the last half of the window) is slightly less in the compensated output. Table 3.1 lists the in-band noise outputs in each channel. While the signal loss averages .8 dB, the noise loss in only .7 dB resulting in a signal-to-noise loss L_{comp} of .1 dB.

Figure 3.9 Match filtered LFM waveforms (Uniform on tranmit, Hamming on receive)

Figure 3.10 Expanded view of compensated matched filter output

3-9
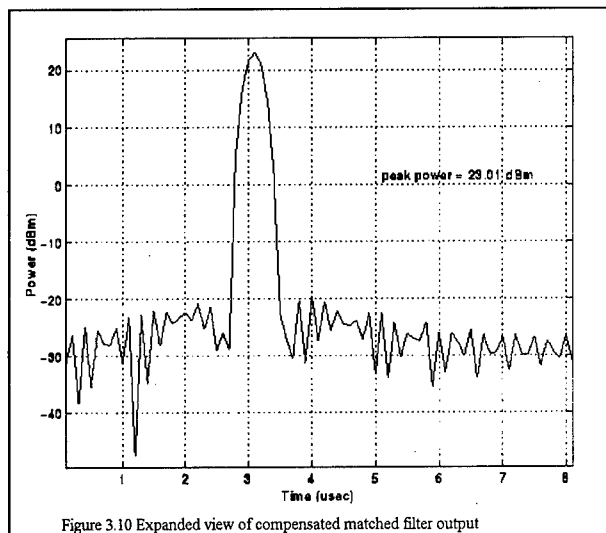
Match filtering uses a filter that is the conjugate of the received signal [32]

$$\chi = S(\omega)H(\omega) = S(\omega)S^*(\omega)$$

and provides the optimum signal-to-noise ratio. When the filter is derived from a weighted or modified version of the signal, the term "match filtering" is still used to describe the process even thought the weighting causes a mismatch. A small mismatch loss is used to represent the additional loss in signal-to-noise ratio.

For pulse compression systems, match filtering provides an improvement in peak signal power and peak signal-to-inband noise ratio. For the uniform weighted case, this maximum improvement is equal to the time-bandwidth product (TB) of the waveform. For non-uniform weightings, a loss of signal-to-noise ratio in the order of 1 to 3 dB will be incurred. In the mismatched case presented in Figures 3.9 and 3.10, the recorded signal is uniformly weighted and the reference signal is Hamming weighted. For the 40 microsecond, 5 MHz waveform used in this example, the maximum improvement in signal-to-noise ratio with uniform weighting is TB = 200 or 23 dB. Hamming weighting provides approximately 1.4 dB of loss [33], resulting in a realized S/N gain of 21.6 dB. Since the weighting was normalized to provide unity noise gain, the expected signal gain is also 21.6 dB, close to the measured signal gain reflected in Figures 3.8 and 3.9. Figure 3.10 presents other results of using the Hamming weighting such as a low sidelobe level (<-40 dB) and a modest increase in pulse width from the uniform weighting case (~250 microseconds vs. 177 microseconds).

For pulse bursts, Doppler processing can provide improvements in signal-to-noise-plus-interference ratio. If s(n) represents the input to the Doppler filter, then the response of filter k centered at $\dfrac{k\omega_o}{N_p}$ can be given as $S(\dfrac{k\omega_0}{N_p}) = \sum\limits_{n=1}^{n=N_p} s(n)wtd(n)e^{-j(n-1)k\omega_0/N_p}$

where wtd(n) represents a weighting function, $\omega_0 = 2\pi f_{prf}$ and f_{prf} is the pulse repetition frequency (prf). The weights wtd are normalized to provide unity noise gain for each filter. Since the noise power is a function of bandwidth and each Doppler filter has a bandwidth in the order of B_n/N_p, the gain (amplification) of each filter is approximately N_p/B_n.

For an N_p pulse train, the gain in signal-to-noise ratio is given by $G_{dop} = N_p / L_{wtd}$ where the L_{wtd}, the loss is signal-to-noise ratio, is given as

Figure 3.11 Response of Doppler filter (uniform weighting)
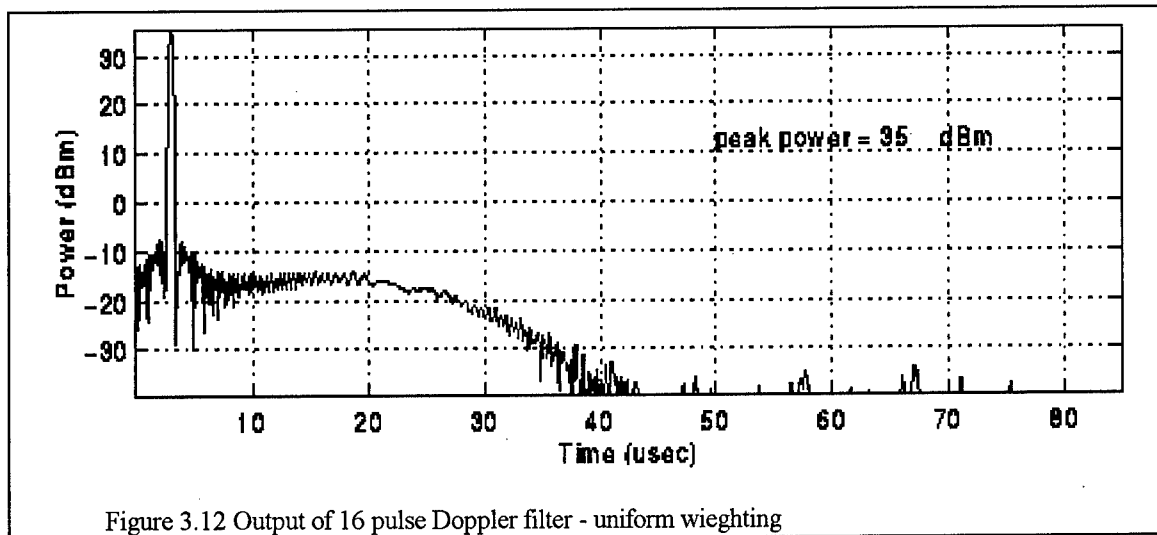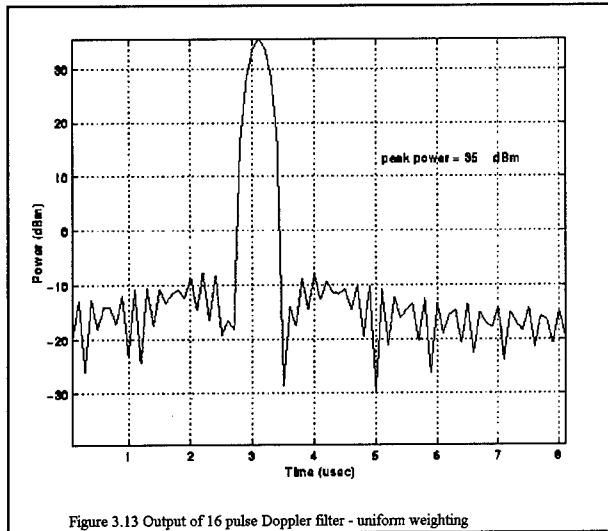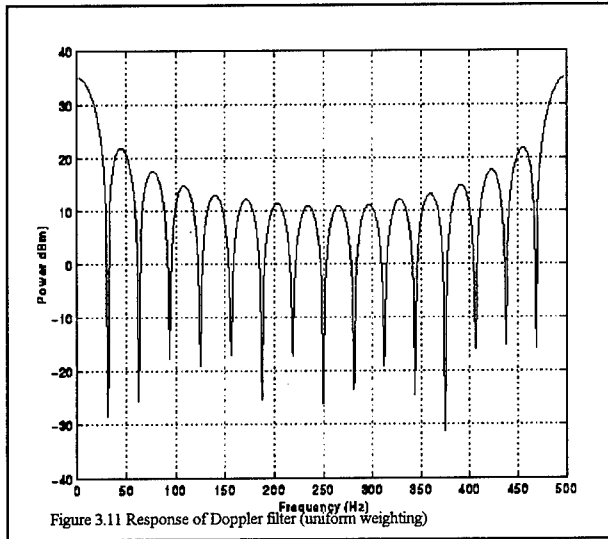
$$L_{wtd} = \frac{Loss_{sig}}{Loss_{noise}} = \frac{\left| \sum\limits_{n=1}^{n=N_p} wtd(n) \right|^2}{\left| \sum\limits_{n=1}^{n=N_p} (wtd(n))^2 \right|}.$$

For uniform weighting, $L_{wtd}=1$ (0 dB) while for popular weightings such as Hamming, Hanning and Blackman, L_{wtd} typically range from 1 to 3 dB. Figures 3.11 through 3.13 present the output of the zero Doppler filter with 16 pulses and normalized uniform weighting. The figures show the expected 12 dB improvement in S/N and signal power. The improvement versus coherent interference is a function of the mean frequency and spread of the interference. For narrow interference such as the return from stationary clutter, the peak gain to null ratio is indicative of the maximum signal-to-noise-plus-interference improvement that the system is capable of. Figure 3.11 shows the measured uniformly weighted filter response for the 16 pulse example. The peak-to-null ratio is over 65 dB.
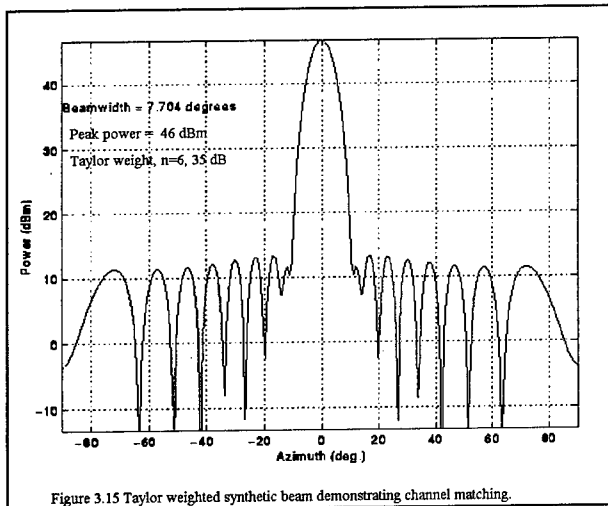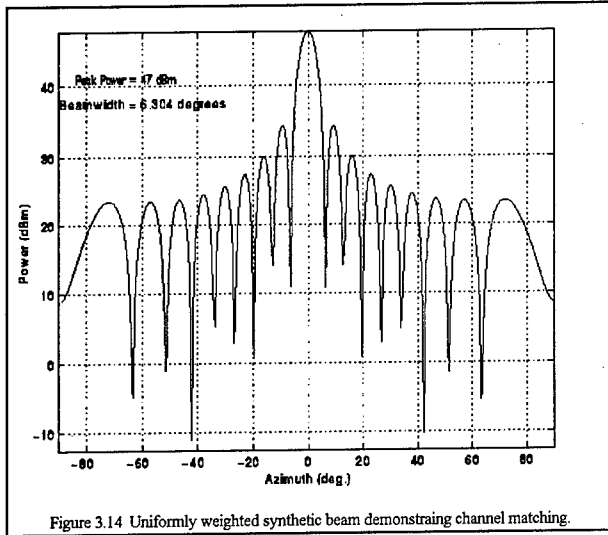

peak power = 35 dBm

Figure 3.13 Output of 16 pulse Doppler filter - uniform weighting

peak power = 35 dBm

Figure 3.12 Output of 16 pulse Doppler filter - uniform wieghting

The final coherent process is azimuth beamforming. The signal power in beam i can be given as

$$S_{beam}(\theta) = S_{input}\left(\sum_{i=1}^{i=16} wta_i e^{j\left(\frac{(2\pi is)\cos\theta}{\lambda}\right)}\right)^2$$

where wta$_i$ is the complex weight to column i and can be represented as $wta_i = |wta_i| e^{-j((2\pi is)\cos\theta/\lambda)}$. The weights used are normalized to provide unity gain to the uncorrelated noise in each channel and a gain of 16*L$_{wta}$ to signals that are correlated within each channel.

The signals used in the current example are calibration signals, not returns received through the array. However, using these signals will demonstrate the effectiveness of the channel-matching procedure and the signal-to-noise gains expected using various array row weightings. Using a wavelength λ of 3.58 inches and a column spacing of 2 inches (.558λ), Figure 3.14 presents the azimuth pattern using a uniform weighting. The power gain of the array weighting is the expected 12 dB. Low sidelobe weighting is often used to reduce the interference from signals outside the mainbeam. One example is the Taylor weighting portrayed in Figures 3.15 and 3.16 where $\bar{n}$ is 6 and the reference peak sidelobe level is 35 dB. The observed signal-to-noise loss L$_{wta}$ of this weighting is approximately 1 dB, close to given theoretical values [33,36]. The estimated beamwidth of 7.7 degrees is 1.22 times the 6.3 degrees obtained for uniform weighting. For both weightings, the sidelobe structure is close to the ideal structure while the peak-to-null ratios are over 58 dB. These values demonstrate that an acceptable degree of channel matching was obtained.

Figure 3.14 Uniformly weighted synthetic beam demonstraing channel matching.

Figure 3.15 Taylor weighted synthetic beam demonstrating channel matching.
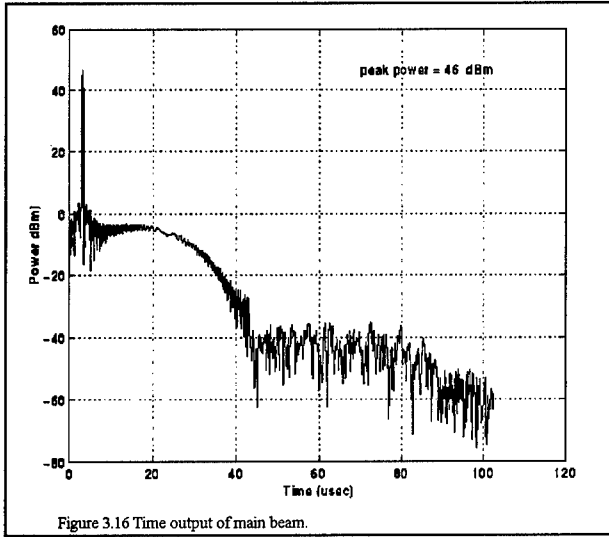
Figure 3.16 Time output of main beam.

Figure 3.16 presents the time output of the main beam. Comparison with Figure 3.12 show that the signal was increased by 11 dB but the noise (beyond 45 usec) is not increased. The noise represents a summation of injected noise, generated by the AWG and the up-converter, and the thermal noise generated by each channel. The injected noise is correlated channel-to-channel and is increased by 11 dB by the beamforming processing. The thermal noise is not correlated channel-to-channel and receives a gain of unity. Since the noise after beamforming shows no significant increase over the noise before beamforming, the noise into the A/D converter is dominated by the thermal noise and other uncorrelated noise sources within each channel.

3.2.3 Array Measurements and Environmental Factors

The closed-loop calibration measurements can not estimate the array parameters not within the loop. These parameters include the column physical aperture A_{col}, the loss of the radome L_{radome}, the average column loss $\overline{L}_{col}$ and the average receiver loss $\overline{L}_r$. A_{col} is one-sixteenth of the physical size of the 16 column antenna or .046 m^2. $\overline{L}_{col}$ includes the inefficiency of the stripline elements and the losses in the stripline, combiners and cables. $\overline{L}_r$ includes the loss of the limiter, rf switch and coupler preceding the preamp. Estimates of these losses require an external known signal. Two methods of providing this external signal are the direct path of the bistatic transmitter and the return from a target of known cross section. Examples of both are provided in the following subsections.

Direct Path Measurements

An estimate of the net value for these losses can be obtained using an external signal such as the transmitter on Tanner Hill. The received signal at each A/D converter can be related to the transmitter and receive parameters by

$$\frac{L_t L_{et} L_{col_i} L_{ri} L_{radome}}{(F_t^2)_i} = \left(\frac{P_t G_t(\theta_t, \phi_t)}{1} \right) \left(\frac{1}{4\pi R_t^2} \right) \left[\left(\frac{A_{col_i}}{S_{AD_i}} \right) \left(\frac{G_{r_i}}{1} \right) \right]$$

3-13

The distance R_t is estimated as 2037 meters from the topographical maps. The peak power of the transmitter P_t was measured as 16.6 mw at the input to the antenna feed. The transmitter antenna was a 10 foot dish with a maximum directive gain of 11100 (40.4 dB) at 3.3 GHz. $\bar{G}_r$ is given in Table 3.1 and other parameters discussed earlier are $A_{col}=.046$ and $N_{col}=16$.

Table 3.2 presents the measured results. The estimated losses show a variation of several dB between the 16 channels. A significant part of this variation is due to a strong azimuth multipath component from large nearby structures. The use of a high gain transmit antenna coupled with the valley floor separating the transmitter and receiver virtually eliminates the presence of a strong specular multipath component from the earth's surface. However, diffuse multipath and reflections from objects near the receiver can cause coherent constructive or destructive interference with the direct signal at the array face, causing an amplitude and phase ripple across the array. The ripple is evident in Figure 3.17 where the column output varies over 2 dB as the receiver is scanned over a 20 degree sector. The dashed lines show the average values that would be expected from the dipole elements in the absence of multipath. The average effect of this azimuth multipath on the average gain of the array F should be close to unity.

A reasonable estimate for the inefficiency of the transmit antenna feed L_t is 1.5 dB and the atmospheric attenuation over a range of 2000 meters is less than .1 dB [22]. Therefore, an estimate of the total receiver loss $L_{radome}L_rL_{col}$ is given in Table 3.2. Since $\bar{L}_r$ has been estimated as 2.2 dB using the manufacturer's data [6], the average loss within the column array and radome is 6.9 dB. The average value of the unknown losses can also be estimated using the
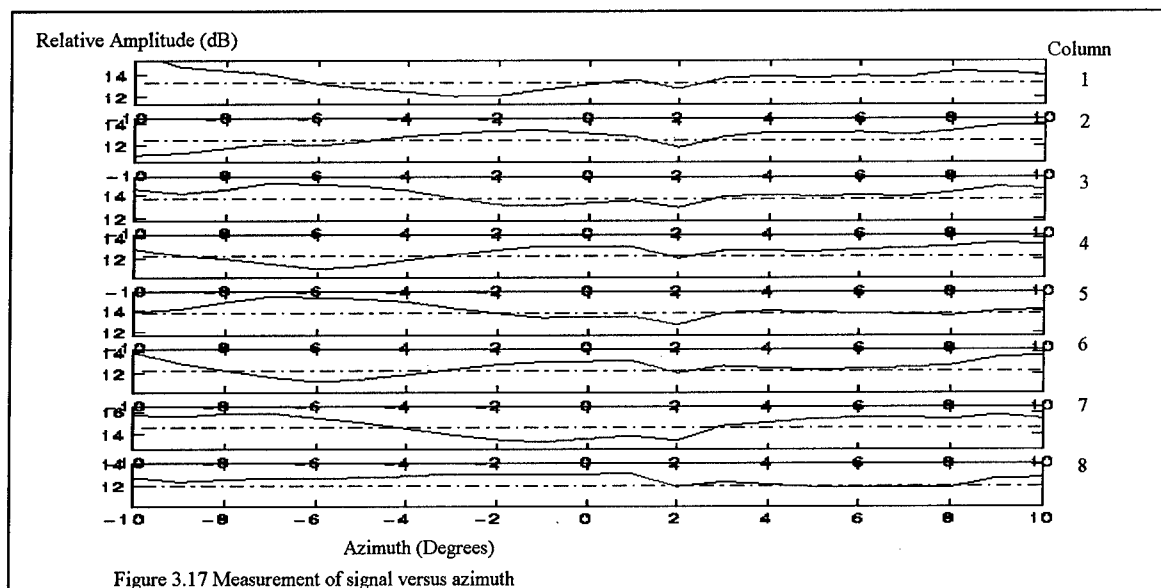

Figure 3.17 Measurement of signal versus azimuth

3-14

Channel	Received Signal (dBm)	Total Losses* (dB)	Estimated $L_{radome}L_rL_{col}$ (dB)
1	+4.9	10.2	8.7
2	+6.3	9.5	8.0
3	+5.7	10.3	8.8
4	+6.6	8.2	6.7
5	+4.8	11.1	9.6
6	+5.6	10.5	9.0
7	+4.7	12.5	11.0
8	+7.3	9.2	7.7
9	+8.1	9.2	7.7
10	+6.1	10.1	8.6
11	+7.1	10.1	8.6
12	+5.4	10.4	8.9
13	+5.5	10.6	9.1
14	+1.3	10.9	9.4
15	+5.9	10.0	8.5
16	+2.0	12.4	10.9
average	5.8	10.6	9.1

Table 3.2 Estimate of unknown RF losses

* includes ~1.5 dB peak ripple due to strong azimuth multipath

** assumes L_r = 2.2 dB, L_t=1.5 dB, F_t = 1

full array processing. The main beam output S can be given by

$$S = \left(\frac{P_t G_t(\theta_t, \phi_t)}{L_t} \right) \left(\frac{\bar{F}_t^2}{4\pi R_t^2 L_{et}} \right) \left[\left(\frac{A_{col}}{\bar{L}_{col} \bar{L}_r L_{radome}} \right) \left(\frac{N_{col}}{L_{wta}} \right) \left(\frac{\bar{G}_r}{L_{comp}} \right) \left(\frac{\wp N_p}{L_{wtr} L_{wtp}} \right) \right].$$

Solving for the unknown losses,

$$\bar{L}_{col}\,\bar{L}_{r}\,L_{radome} = \left(\frac{P_{t}G_{t}}{L_{t}}\right)\left(\frac{F_{t}^{2}}{4\pi R_{t}^{2}L_{et}}\right)\left[\left(\frac{A_{col}}{S_{b}}\right)\left(\frac{N_{col}}{L_{wta}}\right)\left(\frac{\bar{G}_{r}}{L_{comp}}\right)\left(\frac{\mathcal{R}N_{p}}{L_{wtr}L_{wtp}}\right)\right]$$

The measurement used a 5 MHz, 40 microsecond LFM waveform resulting in $\mathcal{R} = 200$. Only one pulse was processed. Uniform weights were used providing $L_{wta}=L_{wtr}=L_{wtp}=1$. Other values are $L_{comp}=1.023$ (.1 dB), $\bar{G}_{t}=53.5$ dB. Using a decibel representation,

$$\left(\bar{L}_{col}\,\bar{L}_{r}\,L_{radome}\right)_{dB} = 12.2 + 40.4 - 1.5 - 11 - 2(33.1) - 13.5 + 12 + 53.5 - .1 + 23 - S$$

$$\left(\bar{L}_{col}\,\bar{L}_{r}\,L_{radome}\right)_{dB} = 48.8 - S.$$

The output, given in Figure 3.18, shows two outputs The larger signal is the signal of interest and has a power S equal to 39.7 dBm resulting in a composite receiver loss of 9.1 dB.

The second signal is caused by internal reflections within the optical cable between the two sites. The presence of the local multipath is also evident in the beam patterns. Figures 3.19 and 3.20 present the antenna patterns using uniform and Taylor weighting, respectively. Strong multipath reflections from the local structures southeast of the receiver is noted between -20 and -40 degrees. Lesser multipath from vegetation can also be noted between +20 and +60 degrees. Figure 3.19 through 3.23 show that these reflections limit to the effective sidelobes of the receiver using non-adaptive weighting to between 25 and 30 dB.

Figure 3.18 Direct signal after match filtering and beamforming. (net gain=35 dB)

Calibration Measurements

Another method of measuring the loss of the receiver is to use a calibrated target located at a known range. During the summer of 1997, measurements were made of the bistatic radar system using a calibrated transponder designed and fabricated at Rome Lab. Details of this calibrator and the results of the experiments are given in another report [35]. A brief description
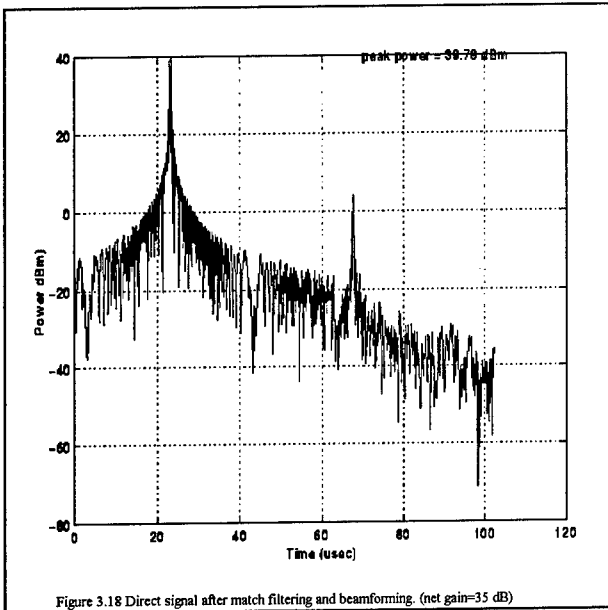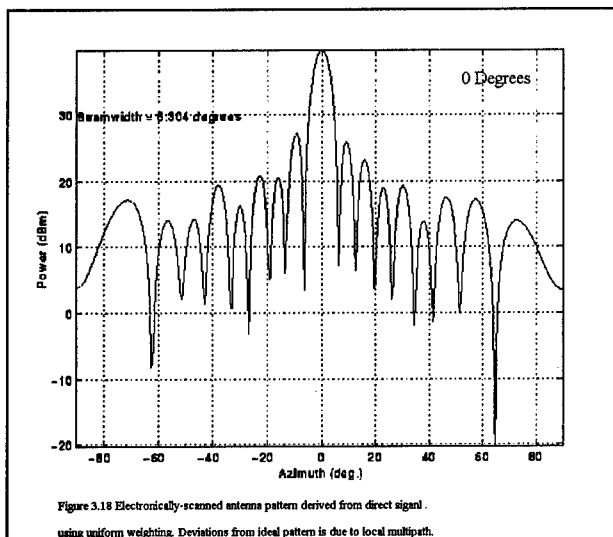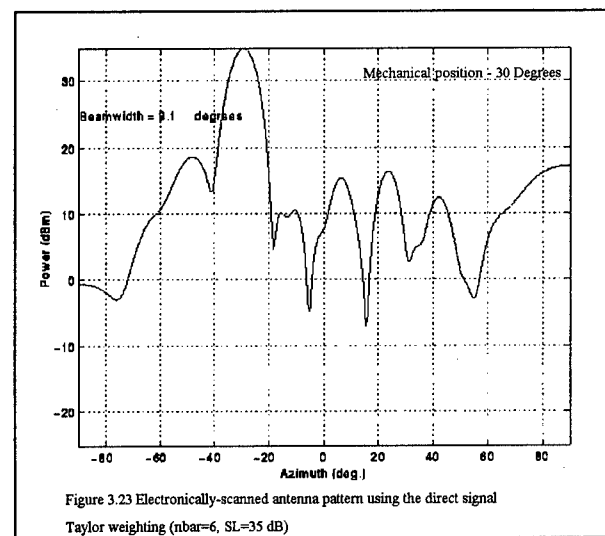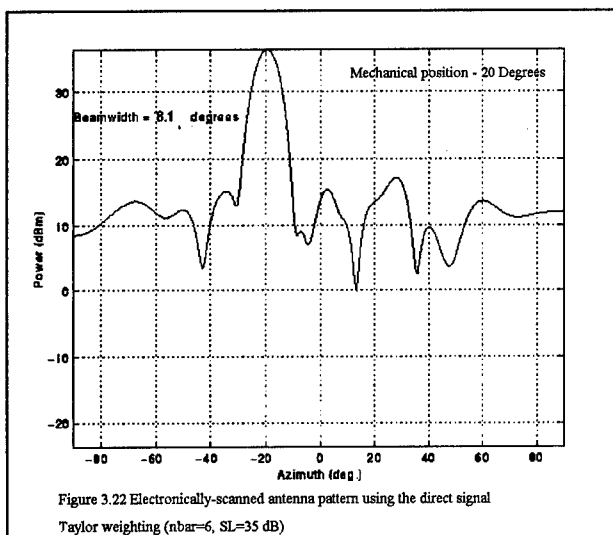
Figure 3.18 Electronically-scanned antenna pattern derived from direct signal. using uniform weighting. Deviations from ideal pattern is due to local multipath.

of this calibrator and the some results defining the system performance is given below.

The calibrated transponder simulates a target of known radar cross section (RCS). If the transmitted energy intercepted by a target can be represented by its aperture in the direction of the transmitter $A(\varphi_t)$ and the gain of the reradiation pattern in the direction of the receiver can be represented by $G(\varphi_r)$, then the RCS of a target can defined as

Figure 3.20 Electronically-scanned antenna pattern using the direct signal using Taylor weighting (nbar=6, SL=35 dB)

Figure 3.21 Electronically-scanned antenna pattern using the direct signal Taylor weighting (nbar=6, SL=35 dB)

Figure 3.22 Electronically-scanned antenna pattern using the direct signal Taylor weighting (nbar=6, SL=35 dB)

Figure 3.23 Electronically-scanned antenna pattern using the direct signal Taylor weighting (nbar=6, SL=35 dB)

$$RCS_{t\arg et}(\varphi_t, \varphi_r) = A(\varphi_t)G(\varphi_r)$$

Calibrated transponders operate in a similar fashion where a range of RCS values can be simulated using gain G_a. With the receive aperture pointed in the direction of the transmitter and transmit aperture pointed at the bistatic receiver,

$$RCS_{transponder} = A_e G_a G$$

The signal can be modulated to distinguish the calibration signal from the surrounding clutter and sophisticated tools are available to provide both amplitude and Doppler modulation simulating target motion [16].

Figure 3.24 shows a block diagram of the calibrated transponder. The receive and transmit aperture was provided using standard gain S-band horns with a gain of 16.5 dB at 3.2 GHz. The effective aperture of each horn can be given as
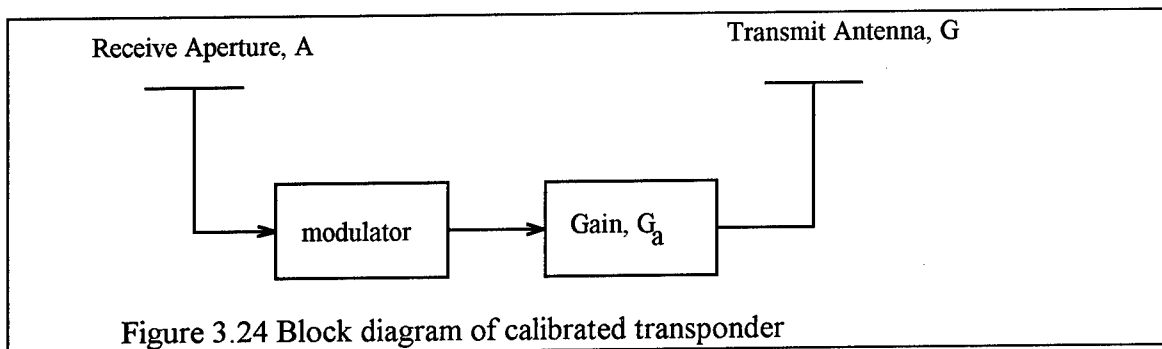
$$A_e = A_{physical}\eta_e = \frac{\lambda^2 G}{4\pi} = \frac{(.094)^2 (44.7)}{12.566} = .031\ m^2\ (-15.1\ dBsm)$$
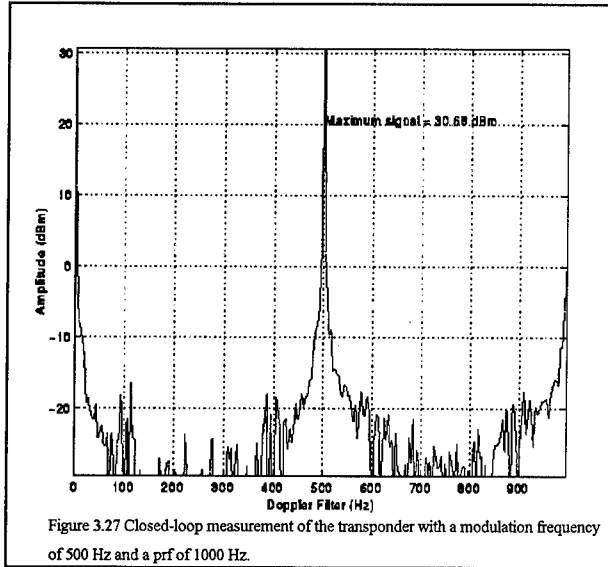
The gain G at the operating frequency of 3.3 GHz. is 16.4 dB. The measured net gain G_a of the modulator, the amplifier and cables is 24 dB for an unmodulated signal. The effective RCS when the no modulation is used is

$$RCS_{dB} = -15.1 + 24 + 16.4 = 25.3\ dBsm\ .$$

The transponder can be used without modulation in a benign clutter environment. However, for field use with the bistatic system, the clutter from the terrain and vegetation within the same resolution cell as the calibrator can easily equal or exceed RCS of 25 dBsm. To use the transponder effectively, modulation must be used to provide a means of discriminating the calibrator signal from the clutter signal.

The modulator is a serradyne device consisting of a 360 degree digital phase shifter and a

Figure 3.24 Block diagram of calibrated transponder

Figure 3.27 Closed-loop measurement of the transponder with a modulation frequency of 500 Hz and a prf of 1000 Hz.

sawtooth digital driver. For an input S-band sinusoidal signal A sin(ωt), the output of an ideal modulator is

$$S_{out} = \frac{A}{2}\cos[\omega t + \phi(\omega_d)]$$

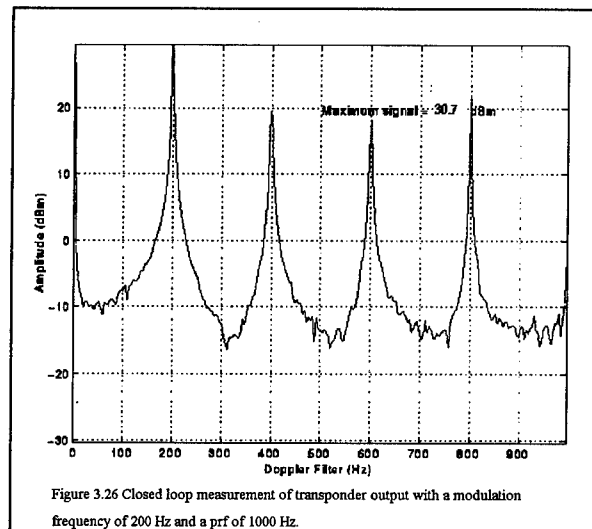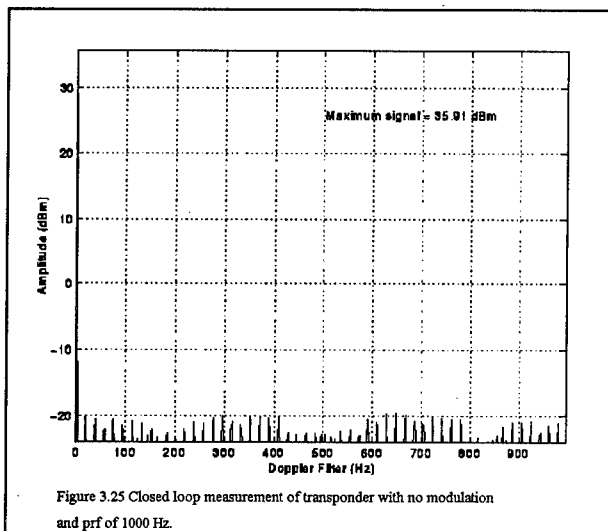where $\phi(\omega_d) = 2\pi x(t)$, x(t) is a periodic sawtooth waveform of period T_d

$$x(t) = \begin{cases} \dfrac{t}{T_{dc}} & \text{for} \quad 0 < t < t_{period} - t_{recover} \\[2mm] 1 - \dfrac{t}{t_{recover}} & \text{for} \quad t_{period} - t_{recover} < t < t_{period} \end{cases}$$

and $f_d = 1/T_d$ is the desired modulation frequency. The amplitude of x(t) is adjusted such that ϕ ranges from -π to +π and T_{dc} is a high percentage of T_d. The spectrum at the output of the modulator will contain a single sideband component of the form

$$S(\omega) = kA\sqrt{RCS}\,S(\omega + \omega_d)$$

where k represents an inefficiency of the modulation.

Nonideal phase shifter performance such as a small amplitude variation as a function of phase and a nonideal sawtooth waveform causes other smaller frequency components as well.

Figure 3.25 Closed loop measurement of transponder with no modulation and prf of 1000 Hz.

Figure 3.26 Closed loop measurement of transponder output with a modulation frequency of 200 Hz and a prf of 1000 Hz.

3-19

Figures 3.25 through 3.27 present closed loop measurements of the transponder output without and with modulation. Figure 3.25 show a DC component is 35.9 dBm with no modulation. In Figures 3.26 and 3.27, the modulated signal is 30.7 dBm, 5.2 dB down. Therefore, when using modulation, the gain G_a is 18.8 dB and the equivalent RCS is 20.1 dB.

Use of the calibrator to check the estimate of system losses requires the use of the radar range equation

$$S = \left(\frac{P_t G_t(\theta_t, \phi_t)}{L_t}\right)\left(\frac{F_t^2}{4\pi R_t^2 L_{et}}\right)\left(\frac{\sigma_t}{1}\right)\left(\frac{F_r^2}{4\pi R_r^2 L_{er}}\right)\left[\left(\frac{\bar{A}_{col} N_{col}}{L_{radome} \bar{L}_{col} L_{wta} \bar{L}_r}\right)\left(\frac{\bar{G}_r}{\bar{L}_{comp}}\right)\left(\frac{\mathcal{R} N_p}{L_{wtr} L_{wtp}}\right)\right]$$

The transponder was placed at a location that was 3720 meters from the high power transmitter and 4157 meters from the receiver. The horns were placed on tripods about 3 feet above the ground. The modulation frequency was set at 250 Hz. The transmit antenna was moved to maximize the transmit gain G_t toward the transponder and the receive antenna was adjusted to -4 degrees elevation to place the receive signal near the peak array response. The azimuth of the receive antenna was ~7 degrees offset from the azimuth of the transponder due to a mechanical limits of the azimuth pedestal. A 40 microsecond LFM waveform using a 2 millisecond PRI was used in the measurement. The processing used was identical to the processing used for the direct signal discussion except that N_p = 16. Uniform weights were used such that L_{wta}=L_{wtp}=L_{wtr}=1. Using the earlier estimate of 9.1 dB for $L_r L_{col} L_{radome}$, the expected value of the received signal can be given as

$S_{dB} = 54.9 + 40.4 - 1.5 - 11 - 2*35.7 + 2*F_t - L_{et} + 20.1 + 2*F_r - L_{er} - 11 - 2*36.2$
$-13.4 + 12 - 9.1 + 53.5 - .1 + 23 + 12$

$$S_{db} = 26.0 \text{ dBm} + 2*F_t - L_{et} + 2*F_r - L_{er}$$

The signal measured in the Doppler filter centered at 250 Hz is presented in Figures 3.28 and 3.29. Substituting the measured power of 26.9 dBm into the above equation, we find the unknown values corresponding to

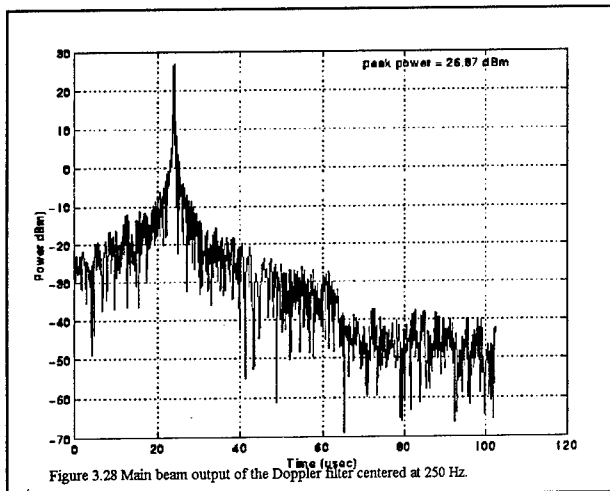$$2*F_t - L_{et} + 2*F_r - L_{er} = 26.0 - 26.9 = 0.9 dB$$

Figure 3.28 Main beam output of the Doppler filter centered at 250 Hz.

The atmospheric attenuation losses L_{et} and L_{er} total less than .1 dB for the short ranges used. Therefore, the result indicates that either the propagation factors provide a net gain, the estimate losses are less than assumed or both. The closeness of the results without examining the propagation factors at each site indicates that the system gains and losses are well characterized. However, the result also demonstrates the necessity of using a calibrated transponder if measurement errors less than 1 dB are required. In the above case, a calibration constant would be established relating the above processing and an output of 26.9 dBm with a 19.1 dBsm target. Then, accurate measurements of other targets placed at or near the calibrator's location can be performed The maximum gain-aperture product of the system is

$$GA_{dB} = 10*\log_{10}\left[\left(\frac{\bar{A}_{col}\,N_{col}}{L_{radome}\,\bar{L}_{col}\,L_{wta}\,\bar{L}_r}\right)\left(\frac{\bar{G}_r}{\bar{L}_{comp}}\right)\left(\frac{RN_p}{L_{wtr}L_{wtp}}\right)\right] = 42.8 + 10\log_{10}\left[\left(\frac{1}{L_{wta}}\right)\left(\frac{RN_p}{L_{wtr}L_{wtp}}\right)\right]$$

and $GA_{db} = 77.8$ dBsm for the example discussed.

With the system noise temperature $T_S = 663°K$ and with knowledge of the signal's bandwidth, the bistatic receiver's sensitivity factor δ can also be defined.

$$\delta = \left[\left(\frac{GA}{G_r L_{comb_n}\kappa\bar{T}_s\,B_n L_{AD}L_{IQ}}\right)\right].$$

Again, for the last example, $L_{A/D}=2.1$ dB, $L_{I/Q} = 3$ dB, $Lcombn=.1$ dB and $B_n = 5$ MHz.

$$\delta = 42.8 + 198.6 - 28.2 - 67 - 2.1 - 3 - 53.5 - .1 + 10\log_{10}\left[\left(\frac{1}{L_{wta}}\right)\left(\frac{RN_p}{L_{wtr}L_{wtp}}\right)\right]$$

$$\delta = 87.5dB + 10\log_{10}\left[\left(\frac{1}{L_{wta}}\right)\left(\frac{RN_p}{L_{wtr}L_{wtp}}\right)\right]$$

The expected signal-to-noise for the last example using R=23 dB and N_p=12 dB is

$$\frac{S}{N} = \left(\frac{P_t G_t}{L_t}\right)\left(\frac{F_t^2}{4\pi R_t^2 L_{et}}\right)\left(\frac{\sigma_t}{1}\right)\left(\frac{F_r^2}{4\pi R_r^2 L_{er}}\right)\delta$$
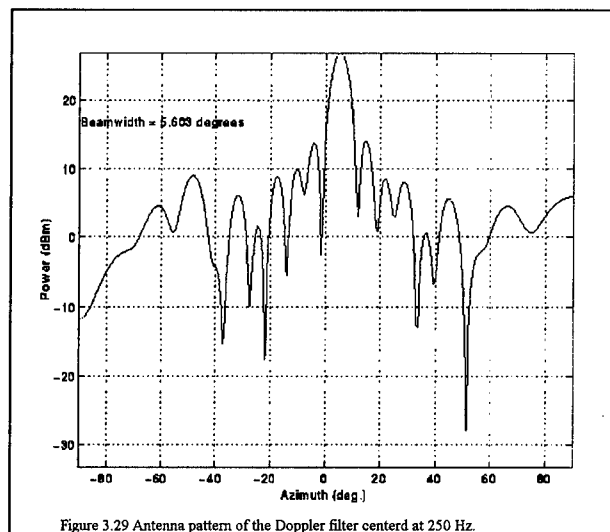

Figure 3.29 Antenna pattern of the Doppler filter centerd at 250 Hz.

$$\frac{S}{N}_{dB} = 54.9 + 40.4 - 1.5 - 11 - 2*35.7 + 19.1 - 11 - 2*36.2 + 122.5$$

$$\frac{S}{N}_{dB} = 69.6dB$$

This value is close to the S/N reflected in Figure 3.28.

4.0 SUGGESTED PROGRAMS AND EXPERIMENTS

The current sensor technology provides the ability to detect and track aircraft, ships, vehicles and even personnel that are within the sensor's direct line of sight and are used in both military and civil surveillance communities. In the civil community, the surveillance is used for monitoring and controlling commercial traffic and for use in anti-crime activity. For the military, this technology provides the means for providing a strategic defense and the accurate assessment of the tactical situation. Satellite and airborne stand-off sensors can detect and track unscreened and visible targets from a safe distance and pass the required information to other assets that can investigate, assess and take the necessary action.

Conversely, there are those who do not wish that their activities be observed and who use techniques to deny this information. Technologies such as stealth have been developed to make the newer threats less visible to the sensors. However, this technology is very expensive and is currently limited to the military of advanced and wealth nations. For other countries or for non-military activities, more conventional methods of reducing effective cross section are used.

One method of long-standing interest to the radar community is the screening of targets by the natural terrain. One example is the intruder who uses the combination of terrain shadowing and the high clutter return of the mountainous areas reduce the probability that his aircraft will be detected. For the military, this intruder could be a cruise missile or terrorist aircraft while for the civil authorities, this intruder could be a smuggler. In either case, an adjunct bistatic receiver can reduce the success of this activity by providing the additional capability and coverage required. By placing the receiver such that the shadowed regions are within the receiver line-of-sight, the intruder is denied the two-way attenuation of the shadowing terrain while the bistatic receiver makes use of the screening attenuation to reduce the clutter at the intruder location.

Another example of screening is the use of vegetation to screen the activities of vehicles and personnel. During the recent war with Iraq, stand-off assets such as JOINT STARS, AWACS or E2C were useful in the detection and tracking of enemy's ground activity. Flying over 50 nm from the area of interest and at altitudes over 30,000 feet, these assets observe the terrain at grazing angles less than 10 degrees.

For open flat terrain, such as the deserts, these assets can detect and track traffic, providing the information to the tactical command. However, in an environment with rough terrain and vegetation, their effectiveness is reduced due to shadowing by the terrain and screening by the

vegetation. The limitation on target detection provided by the backscatter from vegetation and terrain is well known. However, the detection is further complicated by the attenuation, distortion and multipath caused by the vegetation canopy. Further work is needed to quantify these limitations and to determine the multistatic and multisensor system approaches that can reduce the effect of vegetation screening.

The following sections propose two programs to address the above problems. The objective of the first program is the development of the information necessary to address the screening vegetation problem. The second proposed program addresses the use of a bistatic receiver to mitigate the terrain screening problem. Each program consists of a series of experiments to obtain the necessary data and, for each program, one experiment using the existing bistatic receiver is described in detail.

4.1 Detection of Targets within a Vegetation Canopy

This program investigates the detection of targets within a vegetation canopy. The issues that must be addressed in this program are the RCS of the targets, the RCS from the vegetation canopy and the two-way propagation of energy within vegetation canopy. The objective of this program is to provide a database for simulation and system analysis and to directly support the development of a system to provide the desired capability to detection, track and neutralize a screened target.

The database must include information on both targets and the masking vegetation. The target database should include the RCS of the targets requires a set of bistatic measurements as a function of frequency and aspect for targets of interest. The frequencies of interest range from the upper VHF frequencies through X-Band.

The database on the masking vegetation must include information of the backscatter from the vegetation and the propagation with the vegetation as a function of vegetation type, health and state of growth, moisture content and wind conditions. The backscatter from the vegetation and terrain includes the radar cross section (RCS) and the normalized RCS, sometimes called σ_o where both terms are considered random variables that are associated with a vegetation type and vary with time, orientation, location, and sensor characteristics.

The propagation within the vegetation canopy can be given as

$$A(v, \omega) = e^{\{\alpha(t) + j\beta(t)\}l}$$

where $\alpha(t)$ is the time-varying attenuation per unit depth into the canopy, amplitude modulation of the canopy, $\beta(t)$ represents the time-varying phase modulation of the canopy and l is the depth into the canopy. As with RCS, $\alpha(t)$ and $\beta(t)$ are considered random variables that are associated with a vegetation type and vary with time, orientation, location and sensor characteristics.

The following experiment uses the existing S-Band bistatic receiver to provide information for this database. Section 4.1.2 discusses how this experiment can be extended.

4.1.1 Simultaneous Bistatic Measurements of S-band Backscatter and Propagation of a Vegetation Canopy

The existing S-Band bistatic system has the capability of providing accurate RCS and spectral information on targets and clutter. With the use of the calibrated transponder, accurate measurements of propagation attenuation and spectra can also be performed. This experiment makes use of both capabilities to provide simultaneous data on the backscatter and propagation of local vegetation.

This experiment investigates the backscatter and propagation of the local forest vegetation around the Newport site. Figure 4.1 presents a topographic of the region around the Newport site. The terrain is consists of a mixed of open farm land and thickly wooded flat lands and hills. The vegetation includes trees (maple, birch and various coniferous varieties) and shrubs and is analogous to the vegetation in other regions of past and potentially future conflict such as Bosnia. It is proposed that measurements performed at the local sites can lead to capabilities useful in the other analogous region.
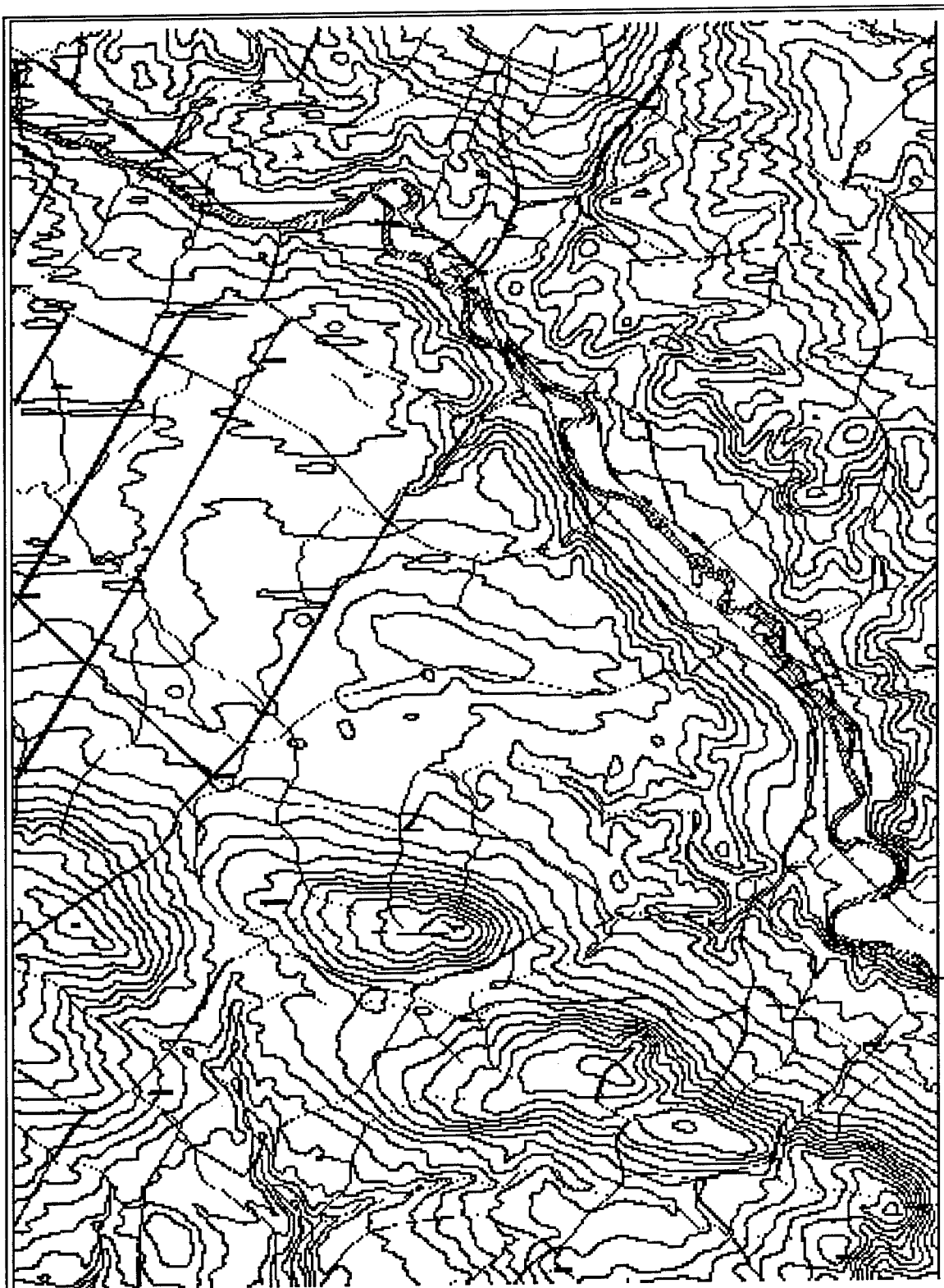
Figure 4.1 Topographic map of the area around the Newport test site.

The experiment involves several tasks. The first task is to obtain data on the simultaneous RCS and propagation of selected areas where vegetation can mask vehicles. The second task is to use the measurement data to predict the detection performance of masked vehicles using conventional techniques and to determine the processing required to obtain improved detection performance. The third task is to perform RCS measurements of available vehicles for use as targets. These targets are then used to perform measurements of moving vehicles traveling through vegetation-screened roadways. These measurements are processed and the detection performance is correlated with that predicted from the RCS and propagation data.

Task 1-Measurements

As shown in Chapter 3, the bistatic receiver can make accurate measurements of the radar cross section of targets and the environment. The bistatic receiver relates the received signal to the RCS of the targets and clutter using the radar range equation

$$S = \left(\frac{P_t G_t(\theta_t, \phi_t)}{L_t} \right) \left(\frac{F_t^2}{4\pi R_t^2 L_{et}} \right) \left(\frac{\sigma_t}{1} \right) \left(\frac{F_r^2}{4\pi R_r^2 L_{er}} \right) \left[\left(\frac{\bar{A}_{col} N_{col}}{L_{radome} \bar{L}_{col} L_{wta} \bar{L}_r} \right) \left(\frac{\bar{G}_r}{\bar{L}_{comp}} \right) \left(\frac{\wp N_p}{L_{wtr} L_{wtp}} \right) \right]$$

$$S = \left(\frac{P_t G_t(\theta_t, \phi_t)}{L_t} \right) \left(\frac{F_t^2}{4\pi R_t^2 L_{et}} \right) \left(\frac{\sigma_t}{1} \right) \left(\frac{F_r^2}{4\pi R_r^2 L_{er}} \right) GA$$

where the gain-aperture product of the receiver was given by

$$GA_{dB} = 10 * \log_{10} \left[\left(\frac{\bar{A}_{col} N_{col}}{L_{radome} \bar{L}_{col} L_{wta} \bar{L}_r} \right) \left(\frac{\bar{G}_r}{\bar{L}_{comp}} \right) \left(\frac{\wp N_p}{L_{wtr} L_{wtp}} \right) \right] = 42.8 + 10\log_{10} \left[\left(\frac{1}{L_{wta}} \right) \left(\frac{\wp N_p}{L_{wtr} L_{wtp}} \right) \right].$$

The use of the calibrated transponder at an unscreened location allows the establishment of a known relationship between known σ_{cal} and a received power S_{cal}

$$S_{cal} = \left(\frac{P_t G_t(\theta_t, \phi_t)}{L_t} \right) \left(\frac{F_t^2}{4\pi R_t^2 L_{et}} \right) \left(\frac{\sigma_{cal}}{1} \right) \left(\frac{F_r^2}{4\pi R_r^2 L_{er}} \right) GA = \frac{\sigma_{cal}}{K_{cal}}.$$

Subsequent measurements of target signals S_t at the same range can then be converted to an equivalent radar cross section σ_t using

$$\sigma_t = K_{cal} S_t.$$

The error in this measurement is a function of the random and bias errors in the measurements. The random errors are dominated by the S/N of the measurement given as

$$\frac{S}{N} = \left(\frac{P_t G_t(\theta_t, \phi_t)}{L_t}\right)\left(\frac{F_t^2}{4\pi R_t^2 L_{et}}\right)\left(\frac{\sigma_t}{1}\right)\left(\frac{F_r^2}{4\pi R_r^2 L_{er}}\right)\delta.$$

where δ is the sensitivity factor of the bistatic receiver

$$\delta = \left[\left(\frac{GA}{G_r L_{comp} \kappa \bar{T}_s B_n L_{AD} L_{IQ}}\right)\right] = 87.5 + 10\log_{10}\left[\left(\frac{1}{L_{wta}}\right)\left(\frac{\wp N_p}{L_{wtr} L_{wtp}}\right)\right]$$

At a range of 4 km, the Newport bistatic system can measure radar cross sections as low as

$$\sigma_t = 3.5 - 10\log_{10}\left[\left(\frac{1}{L_{wta}}\right)\left(\frac{\wp N_p}{L_{wtr} L_{wtp}}\right)\right] \text{ dBsm}$$

with a random error of 1 dB. With modest pulse compression ratios of 23 dB and integration factors of 12 dB, the lower measurement threshold can easily be less than -30 dBsm while the instantaneous dynamic range allows simultaneous accurate measurement of targets and clutter over 43 dBsm. Longer integration intervals such as those used to investigate the spectrum of the clutter return can extend the systems sensitivity by an additional 10 to 20 dB.

As discussed in [7], the bias errors can be complicated and difficult to quantify if the possible bias errors in each term are addressed. For measurements of a point target or a single range cell, the use of the calibrated transponder reduces this error to the bias error to the transponder's gain-RCS relationship and the differences in multipath between the target and the calibrator location. When the calibration constant is formed by averaging over the multipath lobing structure such that $F_r=F_t=1$, the bias error can be made arbitrarily small through accurate measurements of the calibrator's response [35[.

Attenuation measurements are performed by measuring the response from the calibrated transponder as it is placed at various depths into the canopy. The measurement of the propagation attenuation can be given as

$$F_t^2 F_r^2 = S_F\left(\frac{L_t}{P_t G_t(\theta_t, \phi_t)}\right)\left(\frac{4\pi R_t^2 L_{et}}{\sigma_{cal}}\right)\left(\frac{4\pi R_r^2 L_{er}}{GA}\right) = S_F \frac{K_{cal}}{\sigma_{cal}}.$$

Using a 19.1 dBsm calibration target and equation (3.x). accurate measurements of $F_t^2 F_r^2$ at a 4 km range can be made down to

$$F_t^2 F_r^2 > -10\log_{10}\left[\left(\frac{1}{L_{wta}}\right)\left(\frac{\Re N_p}{L_{wtr}L_{wtp}}\right)\right]$$

For $\Re = 100$ and $N_p = 16$ given earlier, two-way attenuation as low as -35 dB can be measured.

The simultaneous recordings of the bistatic cross section and the attenuation must be taken with thought to the analysis that is to be performed. The clutter backscatter is described by its radar cross section RCS or normalized radar cross section NRCS that are usually treated as random variables. Therefore, the data must allow the estimates of mean values, the standard deviation and distribution of the amplitude fluctuation and the correlation and spectral properties of the amplitude and phase fluctuations.

Similarly, the propagation factors $F_t^2 F_r^2$ can also be treated as a random variable with similar statistics concerning mean values, fluctuation statistics and correlation properties. Furthermore, since the measurements are performed simultaneously, the processing must adequately prevent the backscatter energy centered about 0 Hz to contaminate the weaker propagation returns centered at a chosen Doppler frequency.

The bistatic system allows up to 512K word measurements to be made continuously before time must be spent dumping the data to a larger storage medium. When measuring a handful of resolution cells, this allows the measurement of over 512 sequential pulses. This large recording size is more than sufficient for estimates of the mean RCS, its amplitude fluctuation statistics and the correlation properties of the backscatter return. It also allows the user to choose N_p to provide the best compromise between the amplitude sensitivity of the propagation estimates and the ability to investigate correlation properties.

In addition to the radar measurements, auxiliary measurements are required to allow the measurements to be transferable to analogous terrains. When the test areas are identified, the vegetation types and sizes must be recorded. During the course of the measurements, the auxiliary data must also include an estimate of the length and density of the vegetation along the line-of-sight with the transmitter and receiver. Since this varies as a function of season, a reassessment of the vegetation density would be required as needed. One possible guide to categorizing the vegetation types is to use the same guidance used by the Defense Mapping Agency (DMA) for their map products. This would allow a simulation or field user to find analogous vegetation in areas of interest.

Other auxiliary data needed is a description of the health and development of the vegetation, whether the vegetation surface is wet or dry and the wind speed and direction during the data collection.

Task 2 - Data analysis

Useful outputs of the data analysis are the statistics of the backscatter and propagation. These outputs would represent new and useful information to the radar community. Examples of other uses for the raw and processed data are databases for system simulations, analysis and demonstration of hot clutter issues and analysis and demonstration of adaptive array techniques.

Other statistics of interest would be the sensitivity of the data to temporal averaging, spatial averaging (resolution cell size), the frequency diversity, diurnal, weather and seasonal changes, wind speed and direction and grazing angle.

The output required during this program is some conclusion as to the processing that would be required to detect the presence of a moving target within the vegetation canopy. If these values are within the ability of the bistatic system capabilities, then plans could be developed for a demonstration using moving vehicles of known RCS.

Task 3 - Detection of Targets within a vegetation canopy

Measurement of vehicle RCS can be performed in a manner similar to the clutter backscatter. The calibrator is used to provide a calibration constant for a measurement location. Then the vehicle is moved to that location and measurements are performed over different aspect angles [19]. The aspect angles of interest can be determined from the geometry of the screened roads with respect to the bistatic transmitter and receiver. The calibrator is then returned to the canopy to serve as a calibrated reference during the detection experiment. The other auxiliary data on the vegetation and wind conditions are repeated to confirm the conditions of the environment.

4.1.2 Other related experiments using other Rome Lab assets

The experiment provides information on the backscatter and propagation within vegetation canopies at S-band.

Also of interest is the performance at lower frequencies where the attenuation through the canopy is expected to be less, but at the expense of reduced resolution. Rome Lab has a transportable L-band/UHF radar that could also be used to perform these measurements [19]. The

preferred approach is to perform the L-Band/UHF measurements simultaneously with the S-band measurements. This would reduce the overhead of collecting the auxiliary data and allow a direct comparison of the S-Band and L-band/UHF results.

The S-band bistatic receiver is current at a fixed location, limiting the range of bistatic angles and geometries that can be measured. However, the S-Band receiver is enclosed within a shelter that can fit on a flat trailer and be transported to other locations. When combined with a generator, this system can be moved to other locations at the Newport site to allow measurements of the same region from a different bistatic angle.

4.2 Target Detection in the Presence of Terrain Shadowing

This program investigates the feasibility of using an adjunct bistatic radar to detect targets in shadowed regions. The issues to be addressed are the one-way and two-way attenuation and correlation properties of the diffracted energy within the shadowed region, the effective RCS of the clutter from the shadowed regions and the S/N+I obtained versus target size and range. The objective of this program is to provide a database for simulation and system analysis and to support the development of an adjunct bistatic sensor.

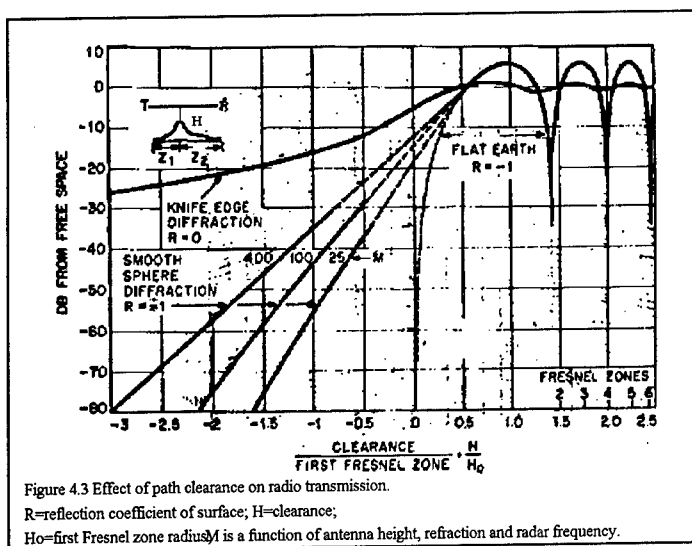The three propagation regions created by the effects of the earth surface are given in Figure

Figure 4.2 Three propagation regions
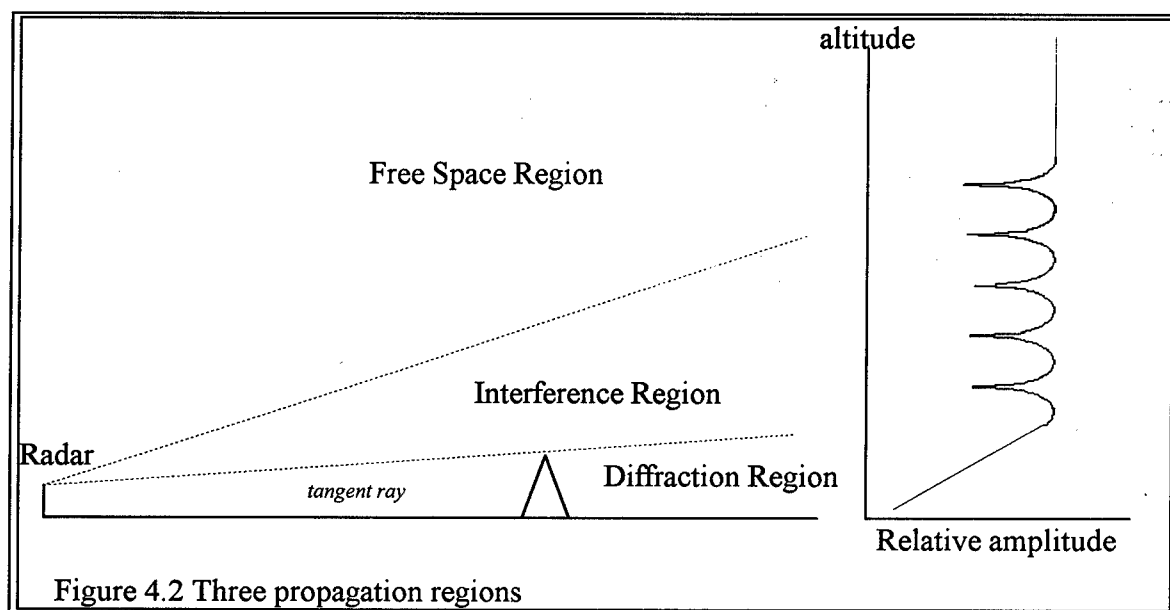
4.2 [14]. The region above the tangent ray is the interference region where multipath from the earth's surface can combine constructive and destructively with the direct signal, creating the characteristic lobing structure well above the tangent ray, the multipath is very weak and the power density is essentially that predicted by free space propagation. The diffraction region is the region below the tangent ray. The power density decreases sharply with altitude below the tangent ray. The propagation loss of the diffracted energy is critically dependent on the radius of curvature of the diffracting edge and the wavelength of the illumination. For knife-edge diffraction where the radius of curvature is small relative to the wavelength, the diffraction loss is minimized. Figure 4.3 presents a nomograph showing the relationship between the relative heights of the diffracting edge and the propagation loss relative to free-space. When the transmitter and the target are at low altitudes relative to the knife edge, a significant loss will occur. However, when the transmitter's altitude is near the height of the knife edge, the one-way propagation loss can be within 20 dB of the free space loss. Furthermore, as the transmitter range from the diffracting edge increases, the diffraction loss is reduced further.

Fortunately, most of the transmitters are usually sited higher than the average terrain to meet coverage requirements. These include the ground-based ARSR-4 systems used to monitor in-route air traffic and the balloon-borne system used by DEA and other Government agencies. For military applications, airborne platforms such as JOINT STARS, AWACS or E2C are used to provide the coverage. Figure 4.4 shows that significant diffracted energy can illuminate the target under such conditions.

Therefore, it is proposed that there is significant diffracted energy in regions where significant shadowing occurs. While the two-way loss may be high enough to significantly reduce the detection probability of screened targets, there may be sufficient energy to allow the use of a bistatic adjunct receiver.

Figure 4.3 Effect of path clearance on radio transmission.
R=reflection coefficient of surface; H=clearance;
Ho=first Fresnel zone radius;M is a function of antenna height, refraction and radar frequency.

Figure 4.2 Knife-edge diffraction loss relative to free space. [15]

4.2.1 Simultaneous measurement of Diffracted S-Band Propagation and Clutter

This experiment measures the S-band propagation loss due to diffraction and effective radar cross section of the clutter resulting from the diffracted energy. The experiment uses a high power transmitter as an illuminator and the bistatic receiver located at the Newport site. The experiment involves two tasks. First, several regions near the Newport site are selected that present a diffraction loss to the transmitter and allow a small controlled test aircraft to fly through. Simultaneous bistatic and monostatic measurements are performed on the diffraction loss using a calibrated transponder as a reference. The clutter from these diffracted regions is also measured. The second task is to analyze the data and assess the system size and the processing that would be required to detect and track a shadowed target through the shadowed regions at several problem sites.
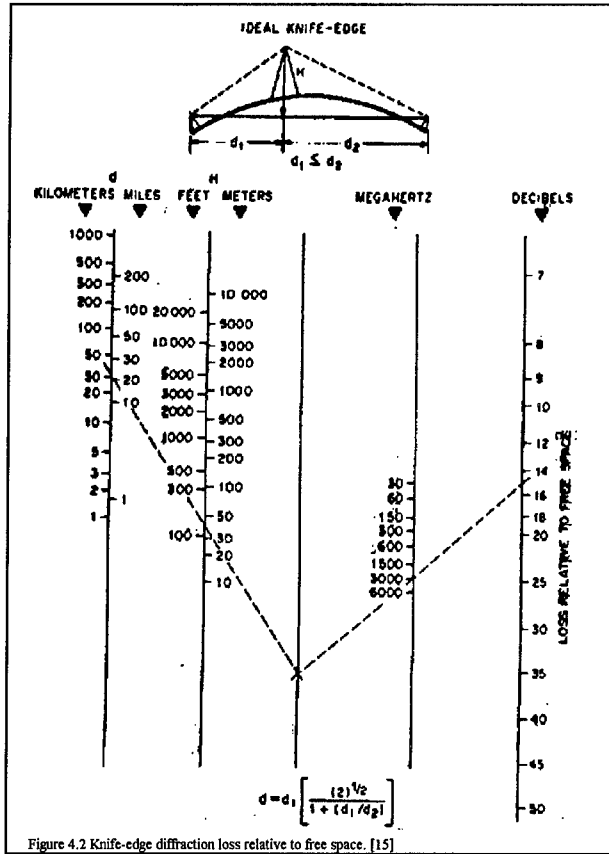
Task 1

The first task is to perform measurements of the propagation loss for selected shadowed regions near the Newport site. As discussed in Chapter 3 and earlier in Chapter 4, the received signal can be related to the propagation loss by

$$S = \left(\frac{P_t G_t(\theta_t, \phi_t)}{L_t}\right)\left(\frac{F_t^2}{4\pi R_t^2 L_{et}}\right)\left(\frac{\sigma_t}{1}\right)\left(\frac{F_r^2}{4\pi R_r^2 L_{er}}\right) GA$$

where the gain-aperture product of the receiver was given by

$$GA_{dB} = 10 * \log_{10}\left[\left(\frac{\bar{A}_{col} N_{col}}{L_{radome} \bar{L}_{col} L_{wta} \bar{L}_r}\right)\left(\frac{\bar{G}_r}{\bar{L}_{comp}}\right)\left(\frac{\mathit{l}N_p}{L_{wtr} L_{wtp}}\right)\right] = 42.8 + 10\log_{10}\left[\left(\frac{1}{L_{wta}}\right)\left(\frac{\mathit{l}N_p}{L_{wtr} L_{wtp}}\right)\right].$$

Two monostatic radars are consisted as possible hosts for this experiment. Rome Lab's S-Band tracking radar has an effective radiated peak power (ERP) of 136 dBm and is located about

31 km from the Newport site. A TPS-75 search radar with comparable ERP would be another candidate system if it is available. Substituting the transmitter parameters and using ranges within 4 km of the Newport site, the signal can be related to the loss by

$$S_{dB} \sim 136 + 2*(F_t) + \sigma_t - 22 - 2*45 - 2*36 + 42.8 + 10\log_{10}\left[\left(\frac{1}{L_{wta}}\right)\left(\frac{\mathcal{R}N_p}{L_{wtr}L_{wtp}}\right)\right] = -5.2 + 2*(F_t) + \sigma_t + 10\log_{10}\left[\left(\frac{1}{L_{wta}}\right)\left(\frac{\mathcal{R}N_p}{L_{wtr}L_{wtp}}\right)\right] \text{dBm}$$

where $F_r \sim 1$ since the region is within the line-of-sight to the bistatic receiver. The random error in the measurement is dominated by the signal-to-noise ratio

$$\frac{S}{N} = \left(\frac{P_t G_t(\theta_t, \phi_t)}{L_t}\right)\left(\frac{F_t^2}{4\pi R_t^2 L_{et}}\right)\left(\frac{\sigma_t}{1}\right)\left(\frac{1}{4\pi R_r^2 L_{er}}\right)\delta.$$

where δ is the sensitivity factor of the bistatic receiver for a 2.5 MHz bandwidth waveform is

$$\delta = \left[\left(\frac{GA}{G_r L_{comp}\kappa \bar{T}_s B_n L_{AD} L_{IQ}}\right)\right] = 90.5 + 10\log_{10}\left[\left(\frac{1}{L_{wta}}\right)\left(\frac{\mathcal{R}N_p}{L_{wtr}L_{wtp}}\right)\right]$$

Substituting,

$$\frac{S}{N}_{dB} \sim 136 + 2*(F_t) + \sigma_t - 22 - 2*45 - 2*36 + 87.5 + 10\log_{10}\left[\left(\frac{1}{L_{wta}}\right)\left(\frac{\mathcal{R}N_p}{L_{wtr}L_{wtp}}\right)\right] = +2*(F_t) + \sigma_t + 39.5 + 10\log_{10}\left[\left(\frac{1}{L_{wta}}\right)\left(\frac{\mathcal{R}N_p}{L_{wtr}L_{wtp}}\right)\right] \text{dB}$$

A similar expression can be developed for the monostatic radar.

$$\frac{S}{N}_{dB\,mono} \sim 136 + 4*(F_t) + \sigma_t - 22 - 4*45 + 118 + 10\log_{10}\left[\left(\frac{1}{L_{wta}}\right)\left(\frac{\mathcal{R}N_p}{L_{wtr}L_{wtp}}\right)\right] = 4*(F_t) + \sigma_t + 52 + 10\log_{10}\left[\left(\frac{1}{L_{wta}}\right)\left(\frac{\mathcal{R}N_p}{L_{wtr}L_{wtp}}\right)\right] \text{dB}$$

These measurements require the probing of the diffraction region with an airborne calibrated transponder. Unlike the directional ground-based transponder currently used by Rome Lab, the airborne transponder must use receive and transmit antennae that are omni-directional in azimuth, but can be directional in the vertical dimension. Such antennae have a gain G in the order of 2-3 dB and an aperture A in the order of .001 m^2. The equivalent RCS of the transponder is given by

$$RCS_{caldB} = A + G_a + G = G_a - 28 \text{ dBsm}$$

By locating the antennas such at least 15 dB of isolation is obtained between them, a net amplification G_a of 38 dB can provide an equivalent cross section of 10 dBsm. Using the tracker's 2.5 MHz, 40 microsecond waveform and a .25 sec (128 pulse) integration and a minimum S/N or 19 dB to provide a 1 dB random error, the bistatic receiver is capable of measuring the transmitter

propagation losses $(F_t)^2_{dB} > -71$ dB. The monostatic radar's measurement ability is limited to $(F_t)^2_{dB} > -42$ dB.

The propagation factor should be treated as a random variable. Therefore, the measurements should be recorded to derive mean values, fluctuation statistics and correlation properties as a function of location below the tangent ray. The bistatic system allows up to 512K word measurements to be made continuously before time must be spent dumping the data to a larger storage medium. When measuring a handful of resolution cells, this allows the measurement of over 512 sequential pulses. This large recording size is more than sufficient for estimates of the mean RCS, its amplitude fluctuation statistics and the correlation properties of the backscatter return. It also allows the user to choose N_p to provide the best compromise between the amplitude sensitivity of the propagation estimates and the ability to investigate correlation properties.

In addition to the propagation loss, the clutter returns competing with the target in the diffracted regions can be recorded and analyzed. The monostatic clutter returns are expected to be very low in amplitude due to the high two-way propagation loss of the energy illuminating the ground. However, the clutter received by the receiver could easily exceed thermal noise and could interfere with zero Doppler or ambiguous returns from the target. Furthermore, the fluctuation statistics of the clutter will represent a convolution of the diffracted propagation and the inherent movement of the vegetation and other ground scatterers. This is expected to decrease the correlation time of the clutter return and decrease the improvement factors obtainable by conventional processing. Such information is needed to determine the effectiveness of bistatic processing techniques.

Other auxiliary data needed is a description of the vegetation at the diffracting edge and the wind speed and direction at the hill tops during the data collection.

The platform used to transport the transponder through the diffraction region is an issue to be resolved. If the platform is an instrumented aircraft or helicopter, an additional benefit can be obtained. Since the transponder uses a single-sideband offset, its return can be separated from the aircraft's return. Therefore, the monostatic and bistatic RCS of the aircraft can be recorded both within the diffraction region as well as in the interference and free-space regions. Simultaneous monostatic and bistatic data on aircraft would be unique. While this data can be used as a baseline data set for the analysis to be perform in the second task, it would also be useful for other uses such as testing theories that derive bistatic RCS from monostatic data.

Other methods that could be used include suspending the calibrator from a manned hot air balloon or using tethered helium-filled balloons.

Task 2 - Analysis

Useful outputs of the data analysis are the statistics of the diffracted bistatic and monostatic propagation and, if available, the bistatic and monostatic cross section of the transponder aircraft. This author is not aware of any propagation and cross section measurements that were performed simultaneously. Therefore, the processed outputs would represent new and useful information to the radar community while the raw data would be useful as a database for system simulations and analysis. The processed data on the propagation factor would include the mean values, fluctuation statistics and correlation properties as a function of location below the tangent ray. Similar information would be derived for the bistatic clutter returns from the diffracted regions.

The output required during this program is some conclusion as to the processing that would be required for bistatic detection of the moving target within the diffraction region. Extension of the data would be applied to other sites where shadowing is a known problem. An experiment would be derived using an existing S-Band search radar and Rome Lab's bistatic receiver to demonstration using an existing search radar.

4.2.2 other related programs and experiments

There are several related programs and experiments that could support the development of an adjunct bistatic receiver. One data set that is required is the simultaneous bistatic/monostatic measurement of aircraft RCS. Currently, bistatic RCS is derived from monostatic data using proposed theory such as the bistatic equivalence theorem [31]. Rome Lab has the S-Band facilities required to perform these measurements and the local commercial and military air traffic provides frequent opportunities to performing these measurements.

Another area of interest is the difference in diffraction propagation statistics when the diffracting edge is hilltop vegetation versus when the diffracting edge is bare. For the measurements that can be performed near Newport, all of the local hilltops contain significant vegetation. This impacts not only the amplitude of the diffracted energy, but also the fluctuation statistics. In the mountainous regions of the western US, the diffracting edge will often be barren, leading to different statistics. Therefore, it would be of interest to repeat the diffraction measurements at mountainous sites.

The experimental bistatic receiver used for the experiments uses off-line or near-real- time processing that can be chosen by an operator. However, an operational bistatic adjunct receiver

will probably be unattended, performing fixed or adaptive processing of the data and transferring the track data to a command center in an automated manner. The existing bistatic receivers can serve as a platform for the development of this automated processing and the associated communication and fusion processing.

5.0 Summary and Conclusions

This report has presented an assessment of the existing bistatic receiver's utility for investigating the clutter phenomenology pertinent to the development of an adjunct bistatic receiver. Measurements of the receiver system were performed using the direct path of a transmitted signal to derive the gains and losses of the bistatic receiver and two characteristic parameters useful for system analysis were derived. First, a gain-aperture product was derived to relate the power density at the face of the array to the processed receiver output.

$$GA_{dB} = 42.8 + 10\log_{10}\left[\left(\frac{1}{L_{wta}}\right)\left(\frac{\Re N_p}{L_{wtr}L_{wtp}}\right)\right].$$

This allows a quick calculation of the receiver performance with a host transmitter using the radar range equation.

$$S = \left(\frac{P_t G_t(\theta_t,\phi_t)}{L_t}\right)\left(\frac{F_t^2}{4\pi R_t^2 L_{et}}\right)\left(\frac{\sigma_t}{1}\right)\left(\frac{F_r^2}{4\pi R_r^2 L_{er}}\right)GA$$

The sensitivity δ of the bistatic receiver was derived to relate the power density at the array to the signal-to-noise ratio of the processed receiver output.

$$\delta = 87.5 + 10\log_{10}\left[\left(\frac{1}{L_{wta}}\right)\left(\frac{\Re N_p}{L_{wtr}L_{wtp}}\right)\right]$$

This allows the analyst to quickly determine the error bounds and detection performance when the array is used with a host transmitter.

Several programs for investigating the clutter and propagation were proposed and two experiments were defined. The first experiment addresses the problem of detecting targets within a vegetation canopy. The experiment provides a method for simultaneously measuring the propagation through the vegetation and clutter backscatter from the vegetation. The output of such an experiment would provide the information needed to determine the effectiveness of using vegetation to screen moving vehicles and other assets and to determine the sensor requirements needed to reduce this effectiveness.

The second proposed experiment addresses the terrain shadowing problem and the potential of using transportable or fixed bistatic adjunct receivers to increase the coverage in the regions illuminated predominately by diffracted energy. An experiment was defined that allows the simultaneous measurement of the bistatic and monostatic propagation characteristics, the bistatic

and monostatic radar cross section of the test aircraft and the bistatic and monostatic clutter return from the diffraction region. Other related experiments were also briefly mentioned.

In conclusion, the existing bistatic receiver has the capability of providing useful information of the clutter phenomenology when used with existing host transmitters. Furthermore, the current system configuration allows the receiver to be easily placed on a transportable platform for use at many locations where clutter and propagation problems are known to exist. This would allow the system can serve as a testbed for the development of a field-implementable adjunct bistatic receiver that can improve the coverage for both military and civilian surveillance systems.

6.0 Bibliography

[1] Wang, H. and Cai, L., "On Adaptive Spatial-Temporal Processing or Airborne Surveillance Radar Systems", IEEE Transctions on Aerospace and Electronic Systems, AES-30, 3 (July 1994), 660-670

[2] Barbarossa, S and Farina, A. "Space-Time-Frequency Processing of Synthetic aperture Radar Signals,", IEEE Transactions on Aerospace and Electronic Systems, AES-30, 2 (April 1994), 341-358

[3] Fante, R. L., "Cancellation of Specular and Diffuse Jammer Multipath Using a hbrid Adaptive Array", IEEE Transactions on Aerospace and Electronic Systems, AES-27, 5 (September 1991), 823-836

[4] Morgan, D. R. and Aridgides, A., "Adaptive Sidelobe cancellation of Wide-Band Multipath Interference", IEEE Transactions Antennas and Propagation, AP-33, August 1995), 908-917

[5] Tang, C. E. T., Liu, K. J. R., and Tretter, S. A., "Optimal Weight Extraction for Adaptive Beamforming Using Systolic Arrays", IEEE Transactions on Aerospace and Electronic Systems, AES-30, 2 (April 1994), 367-384

[6] Simkins, W. L., Multichannel Receiver Characterization for Adaptive Array Applications, Phase 1: Characterization of the Bistatic Receiver Testbed, Dec. 1995

[7] Simkins, W. L., Multichannel Receiver Characterization for Adaptive Array Applications, Phase 2: Algorithms for Calibration of the Bistatic Radar Testbed, April, 1997

[8] Private Communication with Mr. Thomas Scatko, RL/OCTM

[9] Test and Measurement Catalog, Test and Measurement Sector, Hewlett-Packard, Santa Clara, CA, 1993

[10] Skolnik, M. I., Introduction to Radar Systems, McGraw-Hill Book Company, New York, 1962

[11] Scheer, J. A. and Kurtz, J. L. (editors), Coherent Radar Performance Estimation, Artech House, Boston, MA, 1993

[12] Theory of Operations for AASR Receiver Subsystem, TSC-H601-PD-008, 20 July, 1989

[13] HP E1429A/B, 20 MSa/s 2-Channel Digitizer, Users Manual, Hewlett Packard June, 1993

[14] Kerr, Donald E., *Propagation of Short Radio Waves*, McGraw-Hill Book Company, Inc., New York, 1951

[15] Bullington, K., "Radio Propagation Fundamentals,", *Bell System Technical Journal*, Vol. 36, no. 3, pp 593-626, 1957

[16] Blake, L. V., A Guide to Basic Pulse-radar Maximum-Range Calculation Part 1-Equations, Definitions, and Aids to Calculations, NRL Report 6930, Dec. 1969, AD701321

[17] Battan, L. J., *Radar Observation of the Atmosphere*, University of Chicago Press, Chicago, 1973

* [18] Simkins, W. L., FAA Clutter Model Upgrade, RADC-TR-90-170, October, 1990

* [19] Simkins, W. L., Clutter Analysis for ADI, RL-TR-95-31, March 1995

[20] Currie, Nicholas, C., *Techniques of Radar Reflectivity Measurement*, Artech House, Inc, 1984

[21] Phase IV Systems, Inc., 3405 Trianna Blvd, Huntsville, AL 35806-4695

[22] Blake, L.V., Antenna and Receiving-System Noise-Temperature Calculations, NRL Report 5668, Sept. 1961, AD265414

[23] Oppenhiem, A.V. and Schafer, R. W., *Digital Signal Processing*, Prentice-Hall, Englewood Cliffs, New Jersey, 1975

[24] Papoulis, A., *Signal Analysis*, McGraw-Hill, New York, New York 1977

[25] Rabiner, L. R., and Gold, B., *Theory and Application of Digital Signal Processing*, Prentice-Hall, Inc., 1975

[26] Ho, K.C., Chan, Y. T., Inkol, R., "A Digital Quadrature Demodulation System," AES-32-4, October, 1996, 1218-1226

[27] Rice, D. W. and Wu, K. H., " Quadrature Sampling with high dynamic range,", AES-18, 4 Nov 1982), 726-739

[28] Ward, H. R., "An optimum filter for direct A/D conversion," AES-27, 56 (Nov. 1991), 883-886

*RADC-TR-90-170 is Distribution limited to DOD & US DOD Contractors only;
RL-TR-95-31 is Distribution limited Critical Technology, US Government Agencies only.

[29] Rader, C. M., " A simple method for sampling in-phase and quadrature components", AES-20, 6 (Nov 1984), 821-824

[30] Mitchell, R. I., " Creating complex signal samples from a band-limited real signal", AES-25, 3 (May 1989(, 425-427

[31] Willis, Nicolas J., *Bistatic Radar*, Technology Service Corporation, Artech House, Norwood, MA, 1991

[32] Cook, C. E., and M. Bernfeld, *Radar Signals-An Introduction to Theory and Applications,* Academic Press, Inc. New York, March, 1967

[33] Nathanson, F. E., *Radar Design Principles,* McGraw-Hill Book Company, 1969

[34] Skolnik, M. I., *Introduction to Radar Systems,* McGraw-Hill Book Company, New York, 1962

[35] Simkins, W. L., Multichannel Receiver Characterization for Adaptive Array Applications, Phase 4: Calibration Procedures/Tests, to be published

[36] Barton, D. K. and Ward, H. R., *Handbook ofRadar Measurement,* Artech House, Inc., 1984

[37] Way, J.B. et al, " Diurnal Change in TRees as Observed by Optical and Microwave Sensors: The EOS Synergism Study", GE-29-6, pp 807-821, 1991

Appendix A Terms and Definitions

$A_e(\theta, \phi)$ = Receive antenna aperture toward elevation ϕ and azimuth θ (meter^2)

A_{col} = effective aperture of a column array

A_{row} = effective aperture of the row dimension created by digital beamforming

B_{coh} = noise bandwidth of a coherent processing interval $\cong \dfrac{L_{wtr_n} B_s}{n_{beam}}$ (Hz)

B_n = noise bandwidth of analog receiver (Hz)

B_s = bandwidth of signal $\leq B_n$ (Hz)

DC = duty cycle $= \dfrac{\tau_u}{T_{pri}}$

$F_t^2(\theta, \phi)$ = transmit propagation pattern

$F_r^2(\theta, \phi)$ = receiver propagation pattern

G_{pc} = pulse compression S / N gain $= \dfrac{L_{wtr_s}}{L_{wtr_n}} B_s \tau_u \approx \dfrac{\tau_u}{\tau_c}$

G_r = Receiver amplication

$G_t(\theta, \phi)$ = Transmit gain at azimuth θ and elevation ϕ relative to the maximum gain at $G_t(0,0)$

L_{wta} = weighting loss in azimuth beamforming

L_e = environment losses

L_{col} = loss within a column array

L_{comp_s} = signal loss in compensation network

L_{comp} = signal - to - noise loss in compensation network

L_p = signal processing losses

L_r = receiver losses

L_t = transmit losses

L_{wta_n} = noise loss of azimuth beamforming weighting

L_{wta_s} = signal loss of azimuth beamforming weighting

L_{wta} = signal - to - noise loss of azimuth beamforming weighting

L_{wtp_n} = noise loss of Doppler filter weighting

L_{wtp_s} = signal loss of Doppler filter weighting

L_{wtp} = signal - to - noise loss of Doppler filter weighting

$L_{wtr\,n}$ = noise loss of pulse compression weighting

$L_{wtr\,s}$ = signal loss of pulse compression weighting

L_{wtr} = signal - to - noise loss of pulse compression weighting

n_{beam} = number of pulses per beam

N_{col} = number of columns

N_p = number of pulses coherently integrated

P_t = Transmitter Peak Power = Average power within the pulse (watts)

$\overline{P_t}$ = average transmit power = (DC) P_t (watts)

$\mathcal{R}$ = match filter response to a single pulse

R_r = Range from the receiver to the target (meters)

R_t = Range from the transmitter to the target (meters)

S = average signal power within the pulse

$S(\omega)$ = signal voltage spectrum (italics used to distinguish from signal power)

T_{beam} = observation time per beam = $n_{beam} T_{pri}$ (seconds)

$T_s(\theta,\phi)$ = System noise temperature in elevation ϕ and azimuth θ (°K)

T_{pri} = pulse repetition interval (sec)

$T_{sc} = \dfrac{T_{beam}\,\Psi}{\Omega}$ = time to scan solid angle Ψ (sec)

$u(t)$ = transmit waveform

$\chi(\tau,\omega_d) = \left. \displaystyle\int_{-\infty}^{\infty} u(x)u^*(\tau+x)e^{j\omega_d x} dx \right/ \chi_n$ = normalized ambiguity function of the burst waveform

where τ and ω_d are offsets from the peak of the burst matched filter response.

$\chi_n = \displaystyle\int_{-\infty}^{\infty} n(x)u^*(\tau+x)e^{j\omega_d x} dx$ = burst matched filter response to noise

ϕ = elevation angle

θ = azimuth angle

η_a = antenna efficiency (uniform weighting)

κ = Boltzmann's constant = $1.38*10^{-23}$ watt $-$ second $/°K$

$\sigma_t(\beta,\varphi,\gamma)$ = Target RCS at bistatic angle β and aspect (φ,γ) (meter^2)

τ_u = uncompressed pulsewidth (sec)

τ_c = compressed pulsewidth (sec)

Ω_t = solid angle of transmit beam (steradians)

Ψ_t = solid angle to be searched by transmitter (steradians)